8-1-1997

Lateral guidance control of a low-speed vehicle

Haydar Sahin

LATERAL GUIDANCE CONTROL OF A LOW-SPEED VEHICLE

by

Haydar Sahin

A Thesis Submitted
in
Partial Fulfillment
of the
Requirements for the

MASTER OF SCIENCE
in
Mechanical Engineering

Approved by:

Professor _____
Dr. Michael P. Hennessey
Thesis Advisor

Professor _____
Dr. Alan Nye
Committee Member

Professor _____
Dr. Mark H. Kempski
Committee Member

Professor _____
Dr. Charles Haines
Department Head

DEPARTMENT OF MECHANICAL ENGINEERING
COLLEGE OF ENGINEERING
ROCHESTER INSTITUTE OF TECHNOLOGY

AUGUST 1997

I, Haydar Sahin, hereby grant permission to the Wallace Library of the Rochester Institute of Technology to reproduce my thesis in whole or in part. Any reproduction will not be for commercial use or profit

August 21, 1997

ACKNOWLEDGEMENTS

I wish to express my appreciation to the my thesis adviser, Dr. Michael P. Hennessey. I feel deeply indebted to him, not only for the guidance and patience, but also for his intellectual support and inspiration during this process that began when I entered the graduate program. He has taught me the value of being relentless in approaching my challenges. To him, I am forever grateful.

Also, I would like to thank the Turkish Republic's Ministry of National Education for sponsoring my MS program in the USA. Similarly, special gratitude goes to the Department Head, Dr. Charles Haines, for keeping my hopes alive to endure the rigors of the program.

Finally, this thesis is dedicated to my family who have taught me that education is the only gold that you can keep forever and no one can take it away from you.

ABSTRACT

This thesis examines the lateral guidance control of a low-speed vehicle. Several topics are studied in detail: (1) vehicle error-state model for lateral guidance based on Ackerman steering and (2) lateral guidance control of a low-speed vehicle using fuzzy logic. Independently written research papers address each topic.

The first paper presents a second order "error-state" kinematic model based on Ackerman steering appropriate for studying the lateral guidance control of *low-speed* vehicles traversing on roads of constant curvature. Lateral guidance control of vehicles is of great interest to the Advanced Vehicle Control Systems (AVCS) Division of the Intelligent Transportation System (ITS) community. Both linear and nonlinear models are derived in detail. The error states considered are the vehicle's lateral error and heading error measured with respect to the instantaneous road centerline tangent. In addition to the derivation, both simulation and experimental results are presented with very good correspondence being achieved.

The second paper investigates the performance of several different controllers used to perform lateral guidance control of a low-speed vehicle described as a linear nonminimum-phase "error-state" bicycle model based on Ackerman steering. Both a conventional type I proportional-integral (PI) controller and a fuzzy logic controller (FLC) are considered. The PI controller is designed using standard techniques and the two-level FLC / PI controller adjusts both proportional and integral feedback control gains around the baseline values based on heuristics and the current conditions as measured by the lateral error. Time-based simulations using MATLAB® / SIMULINK® permit a comparison between both controllers for several different simulation scenarios of interest. Primary performance metrics considered were percent overshoot and settling time in response to a step input. In general, the two-level FLC / PI controller performed better; 6 % reduction in overshoot and 21 % reduction in settling time.

Vehicle Error-State Model for Lateral Guidance Based on Ackerman Steering

by

Haydar Sahin
Department of Mechanical Engineering
College of Engineering
Rochester Institute of Technology
Rochester, New York

August 1997

ABSTRACT

This paper presents a second order "error-state" kinematic model based on Ackerman steering appropriate for studying the lateral guidance control of *low-speed* vehicles traversing on roads of constant curvature. Lateral guidance control of vehicles is of great interest to the Advanced Vehicle Control Systems (AVCS) Division of the Intelligent Transportation System (ITS) community. Both linear and nonlinear models are derived in detail. The error states considered are the vehicle's lateral error and heading error measured with respect to the instantaneous road centerline tangent. In addition to the derivation, both simulation and experimental results are presented with very good correspondence being achieved.

Vehicle Error-State Model for Lateral Guidance Based on Ackerman Steering

TABLE OF CONTENTS

NOMENCLATURE

POINTS IN SPACE

O	Point representing the center of road curvature
O_v	Point representing the center of vehicle's curvature based on Ackerman steering model
P	Point representing the vehicle's center of gravity (CG) at time t
P'	Point representing the CG at time $t + \Delta t$
P_1	Point representing the center of the front wheel at time t
P_1'	Point representing the center of the front wheel at time $t + \Delta t$
P_2	Point representing the center of the rear wheel at time t
P_2'	Point representing the center of the rear wheel at time $t + \Delta t$

PARAMETERS

L	Distance between axles: $l_1 + l_2$ [m]
l_1	Distance from CG to the front axle [m]
l_2	Distance from CG to the rear axle [m]
R	Radius of road centerline curvature [m]
r	Radius of tires [m]
V	Longitudinal vehicle speed, measured at the rear axle [m / sec]
ω	Angular velocity of vehicle about O_v [rad / sec]

VARIABLES

δ	Front wheel steering angle [deg or rad]
$\varepsilon(t)$	Vehicle heading error at time t [deg or rad]
$\varepsilon(t + \Delta t)$	Vehicle heading error at time $t + \Delta t$ [deg or rad]
$\Delta \varepsilon$	Heading error change: $\varepsilon(t + \Delta t) - \varepsilon(t)$ [deg or rad]
ϕ	Ackerman rotation angle [rad]
t	Time [sec]
Δt	Time increment [sec]

x	Coordinate axis pointing from O to P
y	Coordinate axis orthogonal to the x axis
$y_r(t)$	Lateral error at time t [m]
$y_r(t + \Delta t)$	Lateral error at time $t + \Delta t$ [m]
Δy_r	Lateral error change: $y_r(t + \Delta t) - y_r(t)$ [m]

1.0 Introduction

Background

Considerable research is underway to automatically control vehicles in order to increase highway throughput or to assist drivers in certain critical safety situations. Much of this work falls under the umbrella of what is referred to as the Autonomous Highway System (AHS) Program and / or the Intelligent Transportation System (ITS) (formerly known as the Intelligent Vehicle Highway System (IVHS)) Program. ITS is divided into two categories which are further sub-divided into a total of six divisions. The first category is technology oriented and is concerned with Advanced Traffic Management Systems (ATMS), Advanced Traveler Information Systems (ATIS), and Advanced Vehicle Control Systems (AVCS). The second category is application oriented and includes Advanced Public Transportation Systems (APTS), Commercial Vehicle Operations (CVO), Advanced Rural Transportation Systems (ARTS), among other areas. In general, advanced technologies applied to ITS have the potential to undo damage caused by past transportation policies by improving air quality, reducing traffic congestion, and minimizing energy use and accidents.

A key component of ITS technology concerns the advanced vehicle control system (AVCS) to be used by each vehicle. In fact, throughout the whole spectrum of ITS, it is perhaps the most technically challenging and costly endeavor. AVCS in turn includes four different areas: (1) Collision Avoidance, (2) Control and Guidance, (3) Communication Systems, and (4) Intermediate Products. Control and Guidance is

divided into two parts: lateral control and longitudinal control (e.g. as in described Frankel et al. (1996)). Lateral guidance control offers opportunities for congestion relief, fuel conservation, reduction in traffic related deaths and injuries, and environmental protection.

A number of organizations throughout the US are actively involved in ITS / AVCS related research. Research is being conducted on the instrumentation of vehicles (e.g. at Virginia Polytechnic University, University of Michigan Transportation Research Institute (UMTRI)) and through use of elaborate simulation software (e.g. NAVLAB at Carnegie Mellon University, and UMTRI). Since it is less expensive to simulate highway systems rather than to build them, precise simulation systems will help researchers examine their systems in a virtual environment. One of the most important and challenging AVCS research problems concerns the development of intelligent control algorithms (e.g. fuzzy logic, neural networks, genetic algorithms, fuzzy model reference learning control). Partners for Advanced Transportation and Highways (PATH), affiliated with the University of California at Berkeley, Ohio State University and the University of Minnesota are examples of organizations actively researching intelligent control algorithms for AVCS.

Research Problem Statement

Today, PATH has perhaps the most advanced research ongoing in the area of lateral guidance control of vehicles, especially for highway applications. At PATH, Peng and Tomizuka (1993) have developed *preview control* for lateral guidance control of

vehicles in highway automation. Hessburg (1994) has successfully applied fuzzy logic, fuzzy model reference learning control, and genetic algorithms to lateral guidance control of a vehicle. Research has been both of a theoretical nature and an experimental nature, applying the algorithms to full-sized test vehicles operating on test tracks where possible.

In both of the above cases the intent is to control vehicles moving at highway speeds, typically 100+ KPH. Although vehicles driving at low speeds are commonplace in rural and urban settings (e.g. streets and parking lots), there has been very little research on lateral guidance control of low-speed vehicles. Clearly, in order to achieve higher speeds, such as on the highway, lower speeds need to be achieved first. Also, restrictions on locations for highways and their high cost makes low-speed controlled vehicles inevitable. Control of low-speed vehicles will integrate highways with rural and urban area roads which will make AVCS possible to some level on all roads. Therefore, as a practical matter, it is not possible to neglect the control of low-speed vehicles. While some autonomous guided vehicle (AGV) related research is relevant, as in Pears and Bumby (1989) where imaginary-line following is considered, more research is needed in the area of *lateral guidance control of low-speed vehicles*, especially for non-holonomic[1] vehicles such as typical cars and trucks.

[1] Non-holonomic, versus holonomic or omni-directional vehicles, for which there is a large body of research, especially regarding control of robotic vehicles in somewhat unstructured low-speed settings. Also, in a non-holonomic vehicle system there are certain directions in which the vehicle can not move without wheel slippage, i.e. sideways.

For controller design purposes it is advantageous to develop models of low-speed vehicles. An advantage of modeling a low-speed vehicle is that it is conceptually simpler than modeling a high speed vehicle. One reason is that the order of the model can be lower (e.g. 2^{nd} order versus 4^{th} order in Peng and Tomizuka (1993), as will be shown). Also, when developing a *dynamic* model certain vehicle parameters must be identified such as the yaw moment of inertia of the vehicle and the cornering stiffness of each tire; this may be difficult to do accurately. Assuming proper steering linkage design, an *Ackerman steering* (e.g. as in Wong (1993)) model is valid at low speeds, in which inertia and velocity effects are ignored and wheel slippage is not allowed[2]. In this instance, a vehicle kinematic model based strictly on geometrical equations can be used. For reference purposes, both Peng and Tomizuka (1993), and O'Brien et al. (1996) used dynamic models when generating locational error-state equations. This is necessary in their work because of the high speeds. On the other hand, the Ackerman steering model, which has been used for decades and recently in the design of medium duty trucks, tractors and nursery straddle vehicles (Miller, 1991; Zang, 1986; Miller, 1985; Young, 1985), is the most convenient approach to use at low speeds.

When developing planar vehicle models it is common to use the so-called "bicycle" model, in which roll effects are neglected. For many situations the bicycle model (Fenton, 1980; Shladover, 1978; Whitcomb, 1956) is sufficiently accurate and

[2] Note that at low speeds there are certain vehicles that by design may not exhibit Ackerman steering characteristics, e.g. vehicles with parallel tandem axles. For discussion purposes these vehicles will be ignored.

has been widely used for control design purposes when considering high speed vehicles. A bicycle model for any realistic vehicle can be produced by uniformly shrinking all axle lengths and tire widths to zero, thereby allowing only one infinitesimally thick wheel per axle. However, there has not been any research on the development of an *error-state bicycle model based on Ackerman steering* that can be applied to the lateral guidance of a vehicle on a road at low speeds. Below, such a model is developed and verified through simulation and experimentation.

2.0 The Error-State Ackerman Steering Model

2.1 Assumptions

To simplify the derivation of the error-state model certain critical assumptions need to be made. These include:

- Dynamic effects are negligible since the vehicle is operating at low speeds.
- A bicycle model is acceptable for simplification of the system.
- The magnitude of the lateral error is typically very small when compared with the reciprocal of the instantaneous road curvature.
- Both the steered wheel angle and the heading error are assumed to be very small as well.

The above assumptions are made to reduce the complexity of the model, making possible a linear model[3] , yet permitting a model of sufficient accuracy for many practical situations.

[3] An abbreviated derivation of the nonlinear model is given in Appendix A. In this model the steered wheel angle, the lateral error, and the heading error need not be small.

2.2 Derivation of the Error-State Ackerman Model

In this section, the error-state model based on Ackerman steering is derived and the error states are explained in detail. Ackerman steering implies that all of the vehicle's tires will only roll, and not slip side-ways as the vehicle negotiates a corner at low speeds. From Fig. 1 it follows that the intersection of the lines that are perpendicular to the front and rear wheels will intersect at one point, the instantaneous center of rotation of the entire vehicle (O_v).

The error states are the lateral error (y_r) and the heading error (ε) of the vehicle[4] The lateral error of the vehicle is defined as the smallest directed distance between a specific point P on the vehicle (such as the center of gravity (CG)) and the road centerline. In addition, the heading error is the angle (counterclockwise is positive) between the vehicle heading and the road centerline tangent. The curvature of the road is assumed to be constant (i.e. 1 / R)[5] . Ideally both errors are zero so that the CG of the vehicle will follow the circular road exactly in the direction indicated. In general of course this will not be the case.

Next, an overview of the error-state Ackerman steering model derivation will be given. To derive the error-state Ackerman steering model it is necessary to examine the

---

[4] For comparison purposes, we have tried to preserve the notation adopted by Peng and Tomizuka (1993), i.e., y_r and ε

[5] If this is not the case one can divide the road centerline into a finite number of segments where the road curvature is approximately constant.

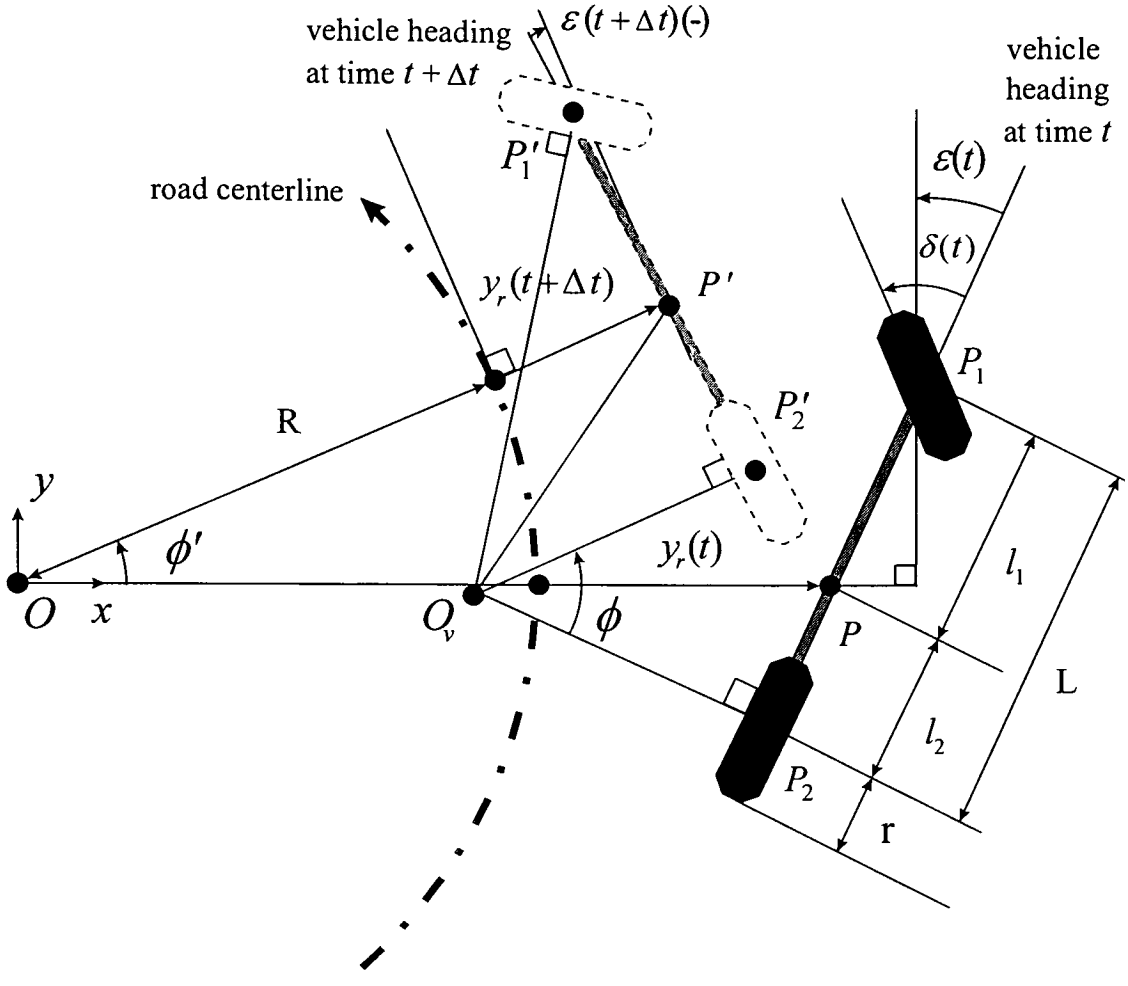

Figure 1 Illustration of lateral error (y_r) and heading error (ε) change based on Ackerman bicycle model and constant radius (R) turn.

location of the vehicle at two different times, time t, and time $t + \Delta t$ where $\Delta t > 0$ is sufficiently small. To facilitate measurement of relative motion, an xy Cartesian coordinate system is utilized as shown. Note that the coordinate frame rotates about point O as the vehicle moves. During the time increment Δt, the vehicle rotates about point O_v through a small angle ϕ[6] with the steered wheel angle δ serving as the input to the system. At time t the lateral and heading errors are observed. Then, at time $t + \Delta t$ the lateral and heading errors are observed again. The difference between the errors at time t and at time $t + \Delta t$ will give us an expression for the error change. By dividing the error changes by Δt and evaluating the limit as $\Delta t \to 0$, the error-state Ackerman steering model is obtained. It consists of one lateral error state equation and one heading error state equation.

[6] Note that we are simplifying matters somewhat by ignoring $\dot{\delta}$ effects, i.e. $|\dot{\delta}|$ is assumed to be sufficiently small when compared to the vehicle's longitudinal speed V, measured at the rear axle.

2.2.1 Lateral Error State Equation

Figure 2 illustrates the location of key points and line segments at time t and at time $t + \Delta t$. Line segment $\overline{P_1 P P_2}$ depicts the vehicle chassis centerline at time t, while $\overline{P_1' P' P_2'}$ depicts the vehicle's chassis centerline at time $t + \Delta t$. Point O_v is the Ackerman turning point, uniquely defined as the intersection of all lines perpendicular to the tire's roll direction, and emanating from the center of each tire. Point O represents the center of the curvature of the road centerline. Note that the vehicle's lateral error y_r is measured with respect to the road centerline at time t.

The problem statement is: given $y_r(t)$, $\varepsilon(t)$, and $\delta(t)$, derive an expression for $y_r(t + \Delta t)$ and evaluate the rate of change of y_r at time t ($\dot{y}_r$) in a limiting sense. The coordinates of point P' are critical to determining $y_r(t + \Delta t)$. The x coordinate of P' can be determined by subtracting $|P'I|$ from the x coordinate of P:

$$x_{P'} = |OP| - |P'I| \tag{1}$$

It follows that $|OP|$ is given by:

$$|OP| = \mathrm{R} + y_r \tag{2}$$

Since $\angle P'PI$ is sufficiently small:

$$|P'I| \cong |P'P|(\angle P'PI) \tag{3}$$

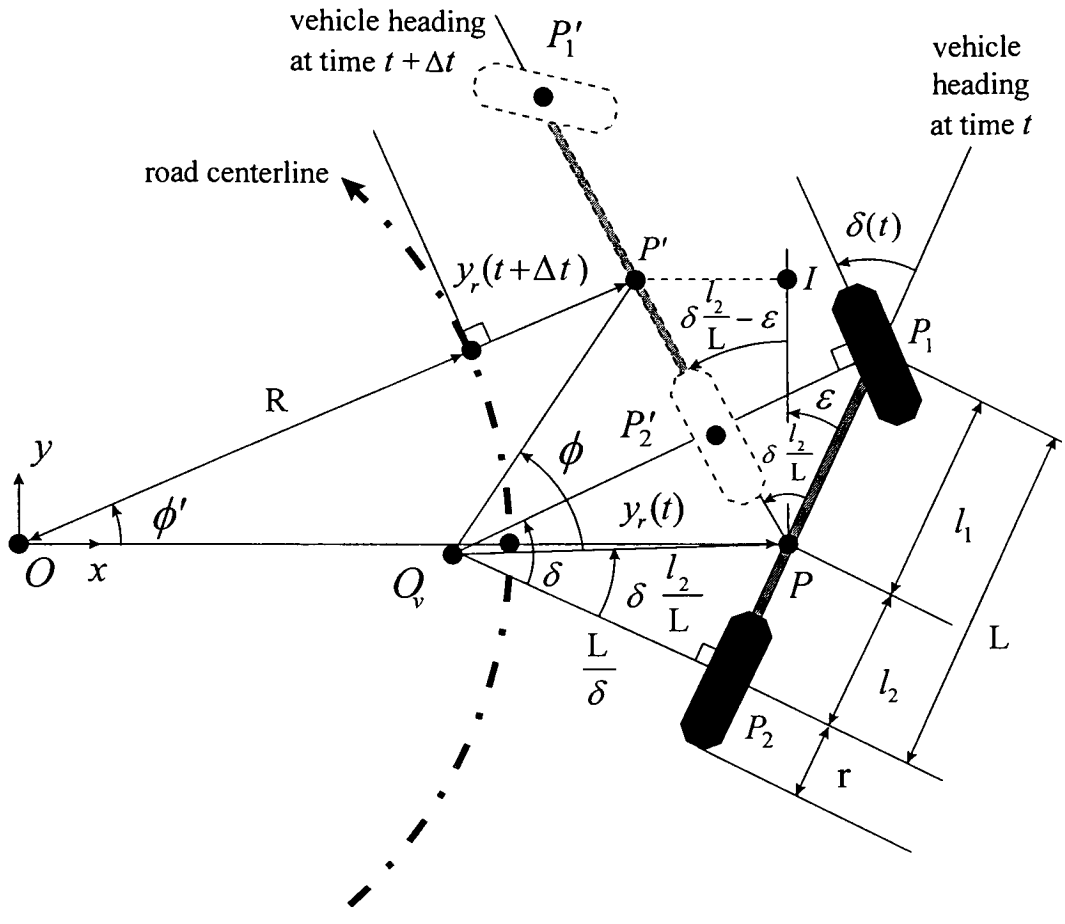

Figure 2 Illustration of lateral error (y_r) change based on Ackerman bicycle model and constant radius (R) turn (small angle assumption).

Thus, through substitution of $|P'I|$, $x_{P'}$ is given by:

$$x_{P'} = |OP| - |PP'|(\angle P'PI) \tag{4}$$

Next, since we are interested in evaluating a limit where Δt is arbitrarily small, we may assume that the Ackerman rotation angle (ϕ) is sufficiently small, such that:

$$|PP'| \cong |O_v P|\phi \tag{5}$$

$$\angle O_v PP' \cong 90 \text{ deg (or } \pi/2 \text{ rad)} \tag{6}$$

Since $\angle P_1 O_v P_2$ is sufficiently small, $|O_v P|$ may be approximated as:

$$|O_v P| \cong |O_v P_2| = \frac{\mathrm{L}}{\tan\delta} \cong \frac{\mathrm{L}}{\delta} \tag{7}$$

Also, using the small angle assumption, $\angle P'PI$ may be approximated as:

$$\angle P'PP_1 \cong \angle PO_v P_2 \cong \delta\frac{l_2}{\mathrm{L}} \tag{8}$$

from which it follows that:

$$\angle P'PI \cong \angle P'PP_1 - \angle IPP_1 \tag{9}$$

Substitution of expressions for $\angle P'PI$, $|OP|$ and $|PP'|$ into Eq. (4) yields:

$$x_{P'} \cong \mathrm{R} + y_r - \frac{\mathrm{L}}{\delta}\phi\left(\delta\frac{l_2}{\mathrm{L}} - \varepsilon\right) \tag{10}$$

Similarly, because of the small angle assumptions, the y coordinate of P' is given by:

$$y_{P'} \cong \phi\frac{\mathrm{L}}{\delta} \tag{11}$$

It remains to find an expression for the Ackerman rotation angle ϕ. It can be parameterized in terms of the vehicle's angular velocity ω and in turn the vehicle's speed V (measured at the rear axle):

$$\phi = \omega \Delta t \cong \frac{V\delta}{\mathrm{L}} \Delta t \tag{12}$$

Substitution of ϕ into Eq. (10) gives:

$$x_{P'} = \mathrm{R} + \left(y_r - \frac{l}{\mathrm{L}}_2 \delta V \Delta t + V \Delta t \varepsilon \right) \equiv \mathrm{R} + \Delta \tag{13}$$

Similarly, substitution of ϕ into Eq. (11) gives:

$$y_{P'} = \frac{\mathrm{L}}{\delta}\left(\frac{V}{\mathrm{L}} \Delta t \delta\right) = V \Delta t \tag{14}$$

The coordinates of point P' have now been evaluated.

Next, the calculation of the lateral error at time $t + \Delta t$ can be formulated as follows:

$$y_r(t + \Delta t) = |OP'| - \mathrm{R} \tag{15}$$

or,

$$y_r(t + \Delta t) = ({x_{P'}}^2 + {y_{P'}}^2)^{1/2} - \mathrm{R} \tag{16}$$

Since in the limit Δt will be arbitrarily small, a Taylor series expansion can be used to simplify the above expression so that:

$$|OP'| = ({x_{P'}}^2 + {y_{P'}}^2)^{1/2} = \mathrm{R}(1 + \Delta_1)^{1/2} \cong \mathrm{R}(1 + \frac{1}{2}\Delta_1) \tag{17}$$

where it remains to determine Δ_1.

Substitution of the above result into Eq. (16) gives:

$$y_r(t+\Delta t) = \left(x_{P'}{}^2 + y_{P'}{}^2 \right)^{1/2} - \mathrm{R} = \mathrm{R}(1+\frac{1}{2}\Delta_1) - \mathrm{R} \cong \frac{\mathrm{R}}{2}\Delta_1 \tag{18}$$

Δ_1 may be evaluated through substitution of Eqs. (13) and (14) into Eq. (17); thus:

$$\frac{V^2(\Delta t)^2}{\mathrm{R}^2} + \left(1+\frac{\Delta}{\mathrm{R}}\right)^2 = 1 + \frac{2\Delta}{\mathrm{R}} + \frac{\Delta^2}{\mathrm{R}^2} + \frac{V^2}{\mathrm{R}^2}(\Delta t)^2 \cong 1 + \Delta_1 \tag{19}$$

If second order terms in Δ and Δt are neglected through linearization in Eq. (19) then Δ_1 is given by:

$$\Delta_1 = \frac{2\Delta}{\mathrm{R}} \tag{20}$$

Substitution of Δ_1 into Eq. (18) yields:

$$y_r(t+\Delta t) = \frac{\mathrm{R}}{2}\Delta_1 = \frac{\mathrm{R}}{2}\left(\frac{2\Delta}{\mathrm{R}}\right) = \Delta \tag{21}$$

We may now evaluate the time derivative of the lateral error as:

$$\dot{y}_r = \lim_{\Delta t \to 0} \frac{y_r(t+\Delta t) - y_r(t)}{\Delta t} \tag{22}$$

Therefore:

$$\dot{y}_r = V\varepsilon - \frac{l_2 V}{\mathrm{L}}\delta \tag{23}$$

2.2.2 Heading Error State Equation

Similarly, we may proceed to derive the heading error state equation. Figure 3 depicts the heading error at time t and at time $t + \Delta t$. The heading error at time $t + \Delta t$ is given by:

$$\varepsilon(t + \Delta t) = \phi' - (\phi - \varepsilon) = \phi' - \phi + \varepsilon \tag{24}$$

or, rewriting in terms of heading error change $\Delta\varepsilon$:

$$\Delta\varepsilon = \varepsilon(t + \Delta t) - \varepsilon(t) = \phi' - \phi \tag{25}$$

The Ackerman rotation angle ϕ was derived previously in Section 2.2.1 as:

$$\phi = \frac{V}{\mathrm{L}}\delta\Delta t \tag{26}$$

From Section 2.2.1 an expression for ϕ' can be determined from:

$$\tan\phi' = \frac{y_{P'}}{x_{P'}} = \frac{V\Delta t}{\mathrm{R} + y_r - \frac{l_2}{\mathrm{L}}V\Delta t\delta + V\Delta t\varepsilon} \tag{27}$$

If the second order terms in the denominator are neglected and a Taylor series expansion is utilized, further simplification is allowed:

$$\tan\phi' = \frac{y_{P'}}{x_{P'}} = \frac{V\Delta t}{\mathrm{R} + y_r} \cong \frac{V\Delta t}{\mathrm{R}}\left(1 - \frac{y_r}{\mathrm{R}}\right) \tag{28}$$

provided $|y_r / \mathrm{R}| < 1$ which is certainly true since $|y_r / \mathrm{R}| << 1$ by assumption. In addition, since by assumption ϕ' will be small, the trigonometric nonlinearity may be eliminated so that:

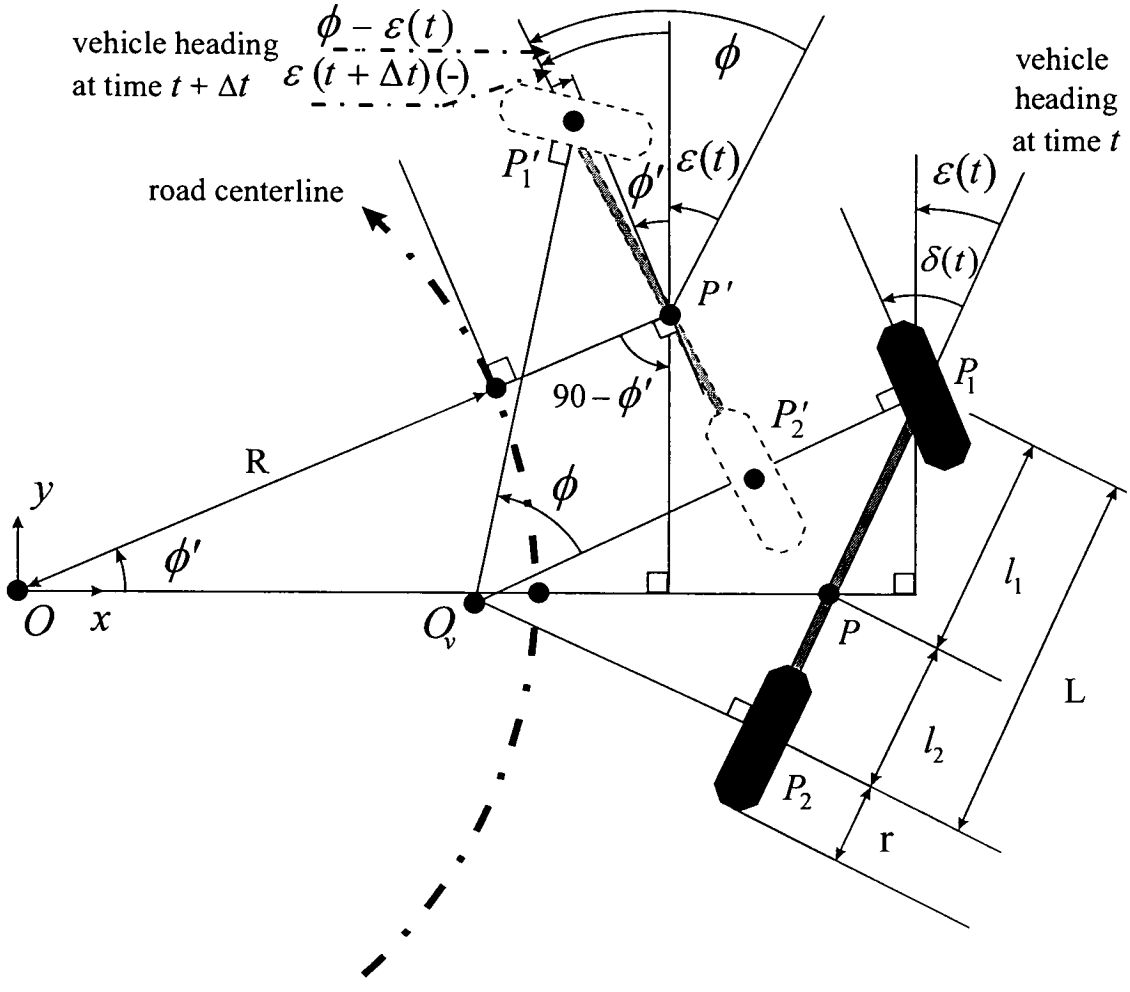

Figure 3 Illustration of heading error (ε) change based on Ackerman bicycle model and constant radius (R) turn (small angle assumption).

$$\phi' \cong \frac{V\Delta t}{R}\left(1-\frac{y_r}{R}\right) \tag{29}$$

Substituting into Eq. (27) yields:

$$\Delta\varepsilon = \frac{V\Delta t}{R}\left(1-\frac{y_r}{R}\right) - \frac{V}{L}\delta\Delta t \tag{30}$$

From the above expression we may evaluate the time derivative of ε as a limit:

$$\dot{\varepsilon} = \lim_{\Delta t\to 0}\frac{\Delta\varepsilon}{\Delta t} \tag{31}$$

to obtain the heading error state equation:

$$\dot{\varepsilon} = -\frac{V}{R^2}y_r - \frac{V}{L}\delta + V\frac{1}{R} \tag{32}$$

2.2.3 Summary

The above derivation produced two linear state equations, one for lateral error y_r and the other for heading error ε. In summary, the Ackerman error-state model is as follows:

Lateral Error State Equation:

$$\dot{y}_r = V\varepsilon - \frac{\frac{l}{2}}{L}V\delta \tag{33}$$

Heading Error State Equation:

$$\dot{\varepsilon} = -\frac{V}{R^2}y_r - \frac{V}{L}\delta + V\frac{1}{R} \tag{34}$$

2.2.4 Interpretation of Special Cases

In the interests of gaining additional insight and providing some corroboration of the model, a number of special cases will be discussed in detail. We will examine the behavior of the system when the steering angle is zero initially (i.e. $\delta(0) = 0$). Both the heading error and lateral error will be monitored through simulation (discussed in more detail below) as time evolves. In addition, we will discuss the implications of the road turning to the right (versus to the left as shown in Figs. 1, 2, and 3), the vehicle turning to the right (versus to the left as shown in Figs. 1, 2, and 3), and the limiting case of a straight road.

Heading Error ($\varepsilon(t)$) Implications When $\delta(t) = 0$: When $\delta(t) = 0$ the model applies in the limit as $\delta \rightarrow 0$ from the right. ε will always be increasing since $\dot{\varepsilon}$ is always positive in Eq. (34); rewriting we have:

$$\dot{\varepsilon} = \frac{V}{\mathrm{R}}(1 - \frac{y_r}{\mathrm{R}}) \tag{35}$$

Observe that the expression $(1 - \frac{y_r}{\mathrm{R}})$ is always positive because $\mathrm{R} \rangle\rangle y_r$. Figures 4, 6, and 8 illustrate how ε increases, regardless of the initial heading error, $\varepsilon(0)$.

Lateral Error ($y_r(t)$) Implications When $\delta(t) = 0$: When $\delta(t) = 0$ three cases need to be considered for Eq. (34):

- $\varepsilon(0) < 0$
- $\varepsilon(0) = 0$
- $\varepsilon(0) > 0$

Let us consider each of these cases in more detail.

a) When $\delta(t) = 0$, $\varepsilon(0) < 0$, $y_r(0) = 0$ from Eq. (33), $\dot{y}_r(0)$ is negative. Therefore, when the initial condition for the heading error is negative, y_r will decrease from its initial value of zero (see Figs. 4 and 5).

b) When $\delta(t) = 0$, $\varepsilon(0) = 0$, $y_r(0) = 0$ from Eq. (34), $\dot{\varepsilon}$ is positive and ε is increasing. Therefore, from Eq. (33), when the initial condition for the heading error is zero, y_r will increase from its initial value of zero (see Figs. 6 and 7).

c) When $\delta(t) = 0$, $\varepsilon(0) > 0$, $y_r(0) = 0$ from Eq. (34), $\dot{\varepsilon}$ is positive and ε is increasing. Therefore, from Eq. (33) when the initial condition for the heading error is positive, $y_r(0)$ will increase from its initial value of zero (see Figs. 8 and 9).

Similar results are obtained when $y_r(0) \neq 0$.

Road Turning to the Right : By a symmetry argument we can redefine a new coordinate system when considering right turns and use the same model developed above with the sign convention noted in Fig. 10.

Vehicle Turning to the Right : It can be shown that the above error-state equations also apply to the case when the vehicle is turning in the opposite direction of the road (i.e. $\delta < 0$). Figure 11 illustrates the problem set-up in this instance.

Straight Road Case : When the road is straight, either of the above cases (i.e. turn right or turn left) applies, but only in a limiting sense, i.e. when $R \rightarrow \infty$. From Eqs. (33) and (34) the error-state model reduces to:

$$\dot{y}_r = - V\varepsilon + \frac{l_2}{L} V\delta \tag{36}$$

$$\dot{\varepsilon} = - \frac{V}{L}\delta \tag{37}$$

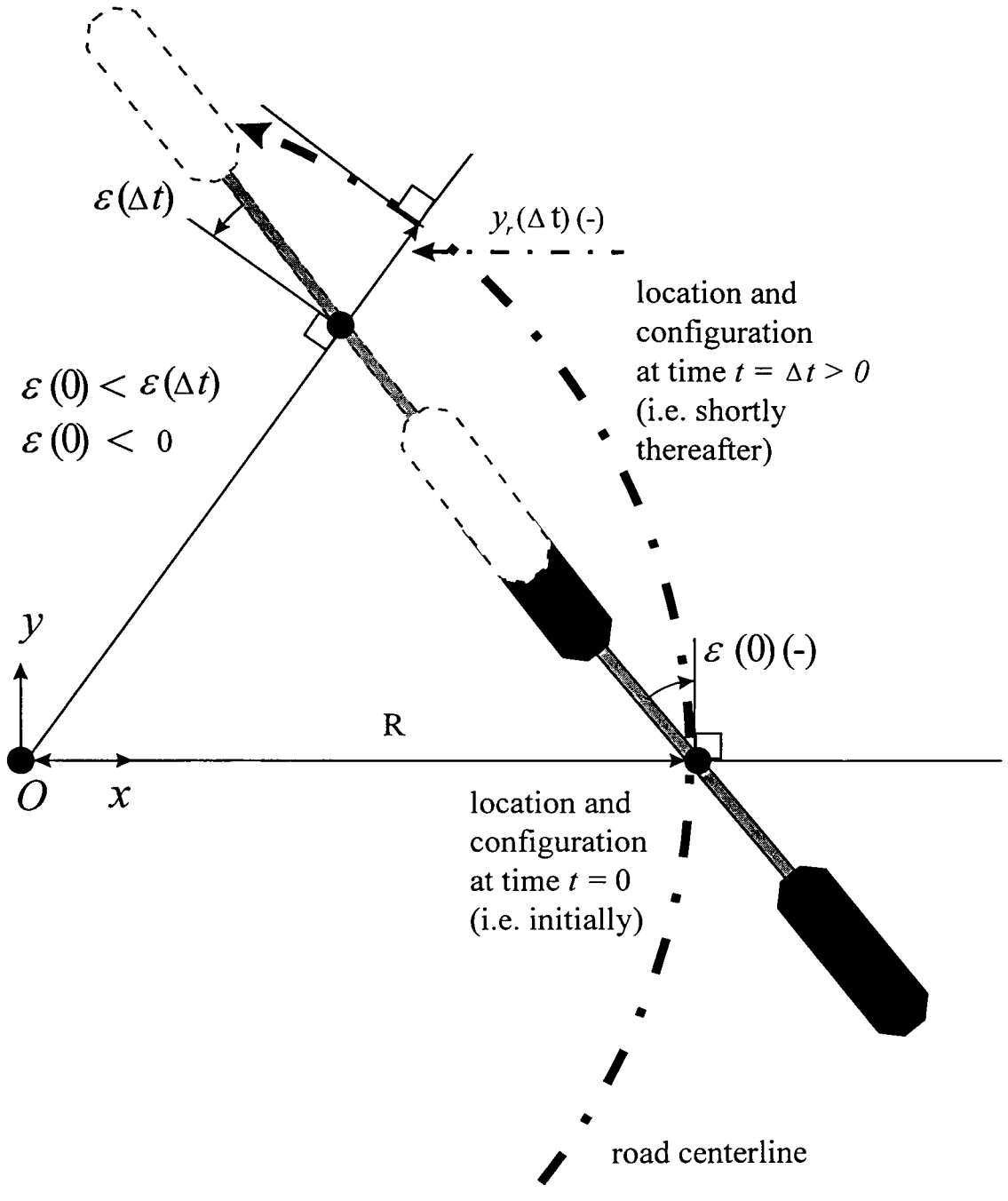

Figure 4 Vehicle locations and configurations when $\delta(0) = 0$, $y_r(0) = 0$, $\varepsilon(0) < 0$ and shortly thereafter (i.e. $t = \Delta t$ with $\delta(t) \equiv 0$). Note: motions have been exaggerated to illustrate the error change effectively.

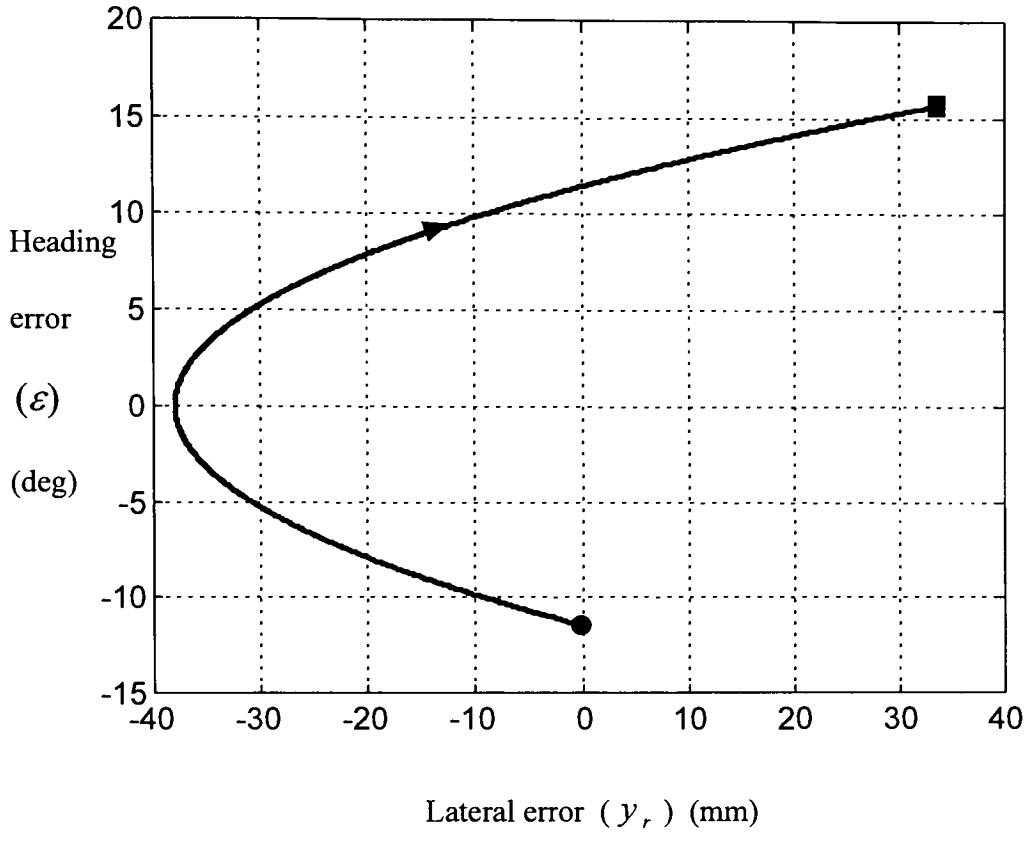

Figure 5 Simulation results when $\delta(0) = 0$, $y_r(0) = 0$, $\varepsilon(0) < 0$, $V = 1.0$ m / sec, L = 0.3 m, $l_2 = 0.12$ m, R = 1.92 m, and $t \in [0\ ,\ 0.9]$ (sec).
Note : (●) represents starting point.
(■) represents approximate end of linear range.

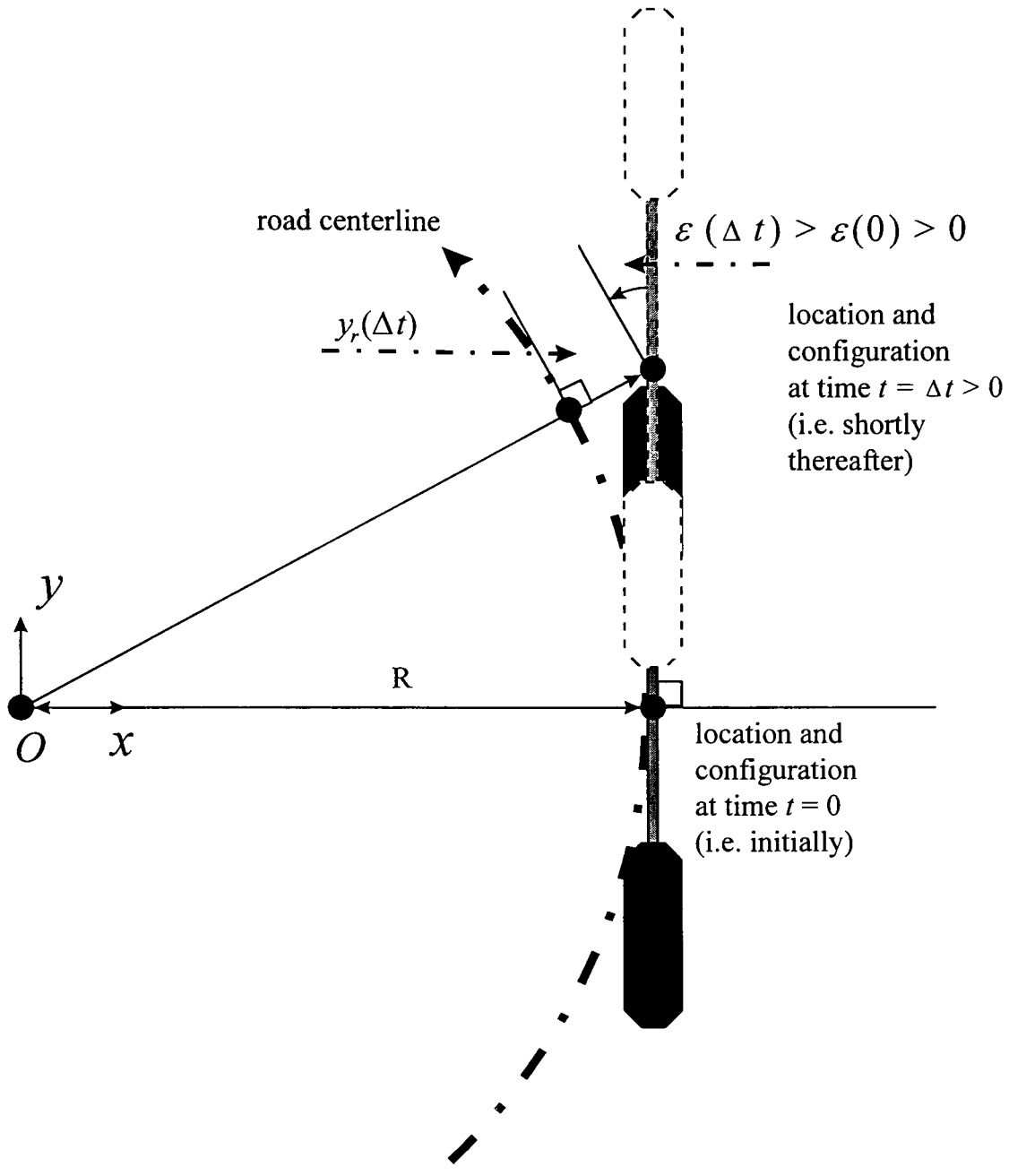

Figure 6 Vehicle locations and configurations when $\delta(0) = 0$, $y_r(0) = 0$, $\varepsilon(0) = 0$, and shortly thereafter (i.e. $t = \Delta t$ with $\delta(t) = 0$). Note: motions have been exaggerated to illustrate the error change more effectively.

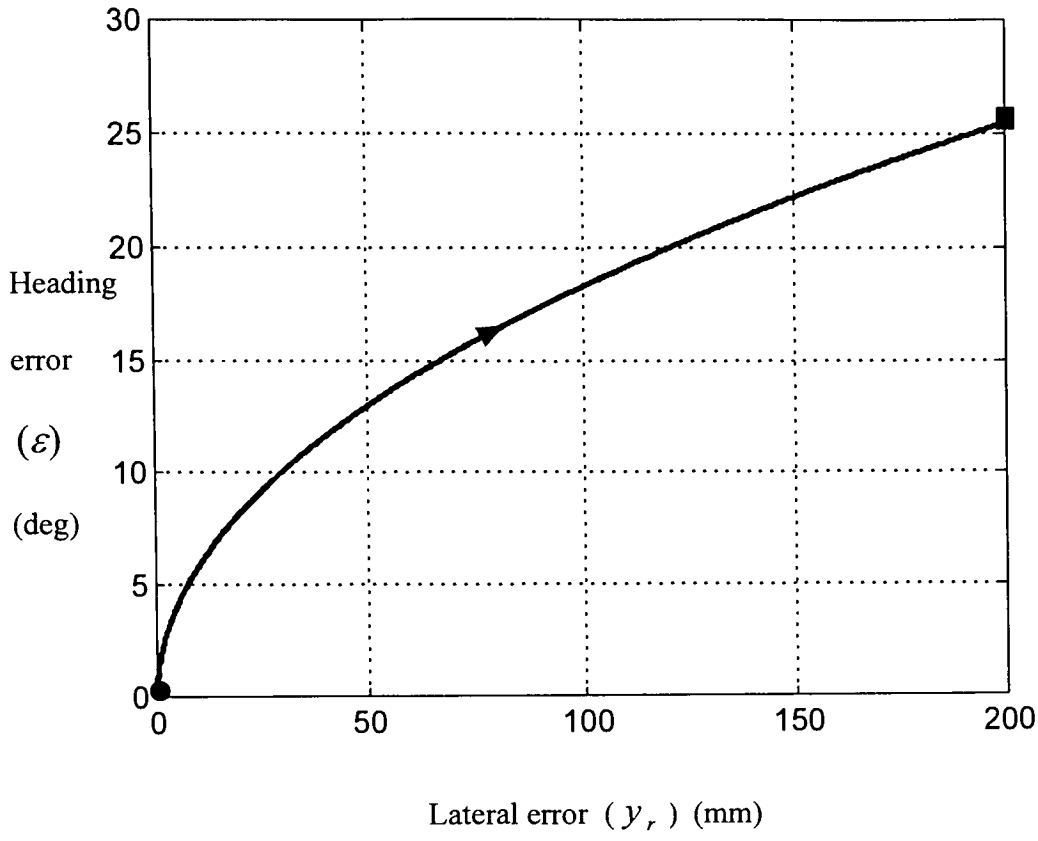

Figure 7 Simulation results when $\delta(0) = 0$, $y_r(0) = 0$, $\varepsilon(0) = 0$, $V = 1.0$ m / sec, L = 0.3 m, $l_2 = 0.12$ m, R = 1.92 m, and $t \in [0, 0.884]$ (sec).
Note : (●) represents starting point.
(■) represents approximate end of linear range.

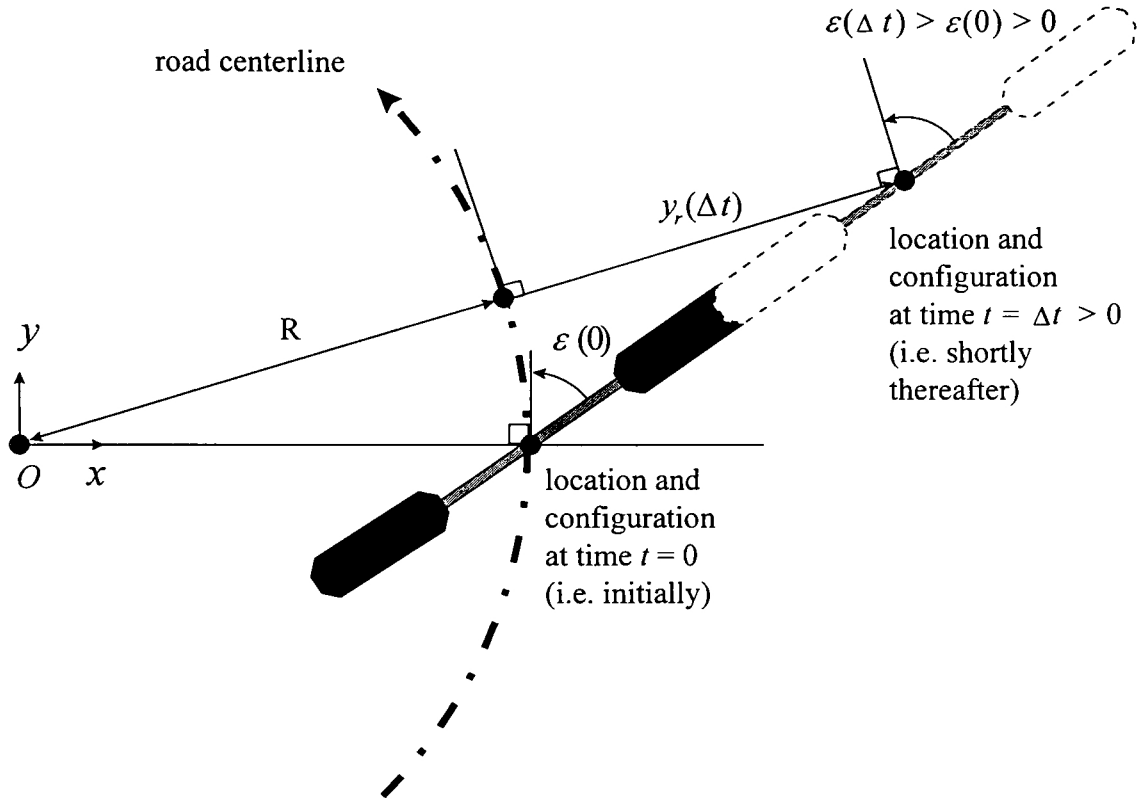

Figure 8 Vehicle locations and configurations when $\delta(0) = 0$, $\varepsilon(0) > 0$, $y_r(0) = 0$, and shortly thereafter (i.e. $t = \Delta t$ with $\delta(t) \equiv 0$). Note: motions have been exaggerated to illustrate the error change more effectively.

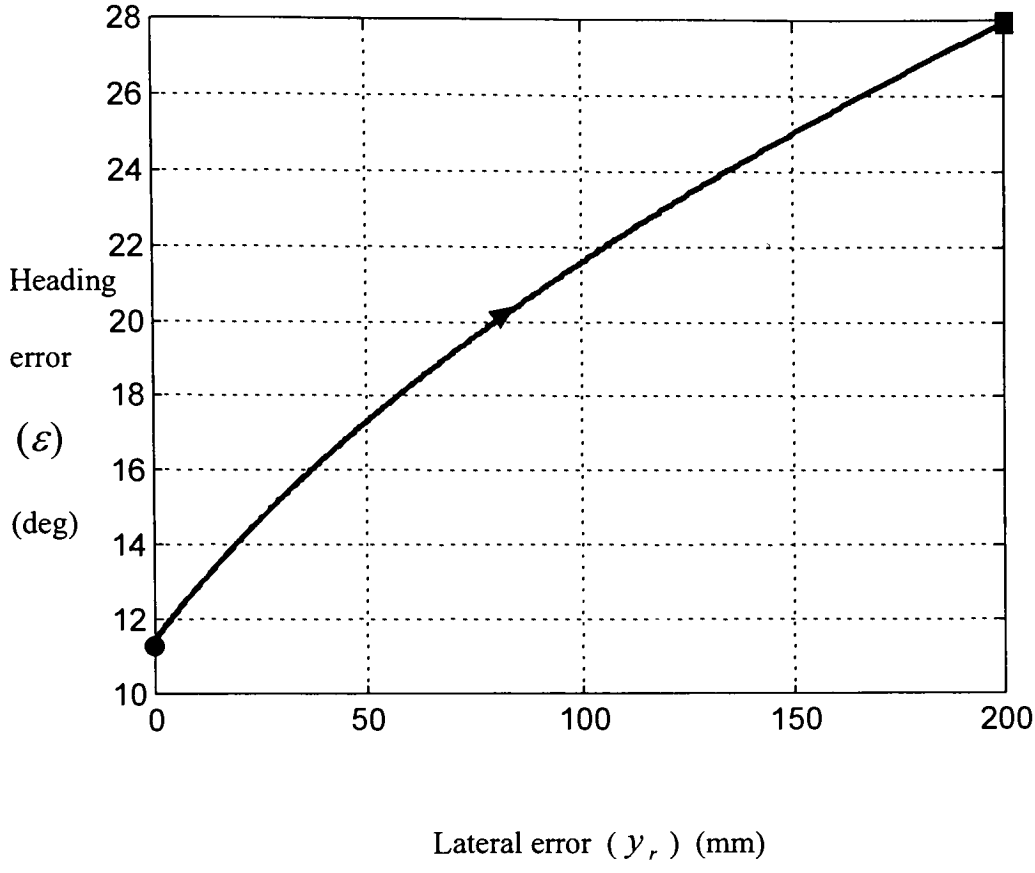

Figure 9 Simulation results when $\delta(0) = 0$, $y_r(0) = 0$, $\varepsilon(0) > 0$, $V = 1.0$ m / sec, L = 0.3 m, $l_2 = 0.12$ m, R = 1.92 m, and $t \in [0\ ,\ 0.576]$ (sec).
Note : (●) represents starting point.
(■) represents approximate end of linear range.

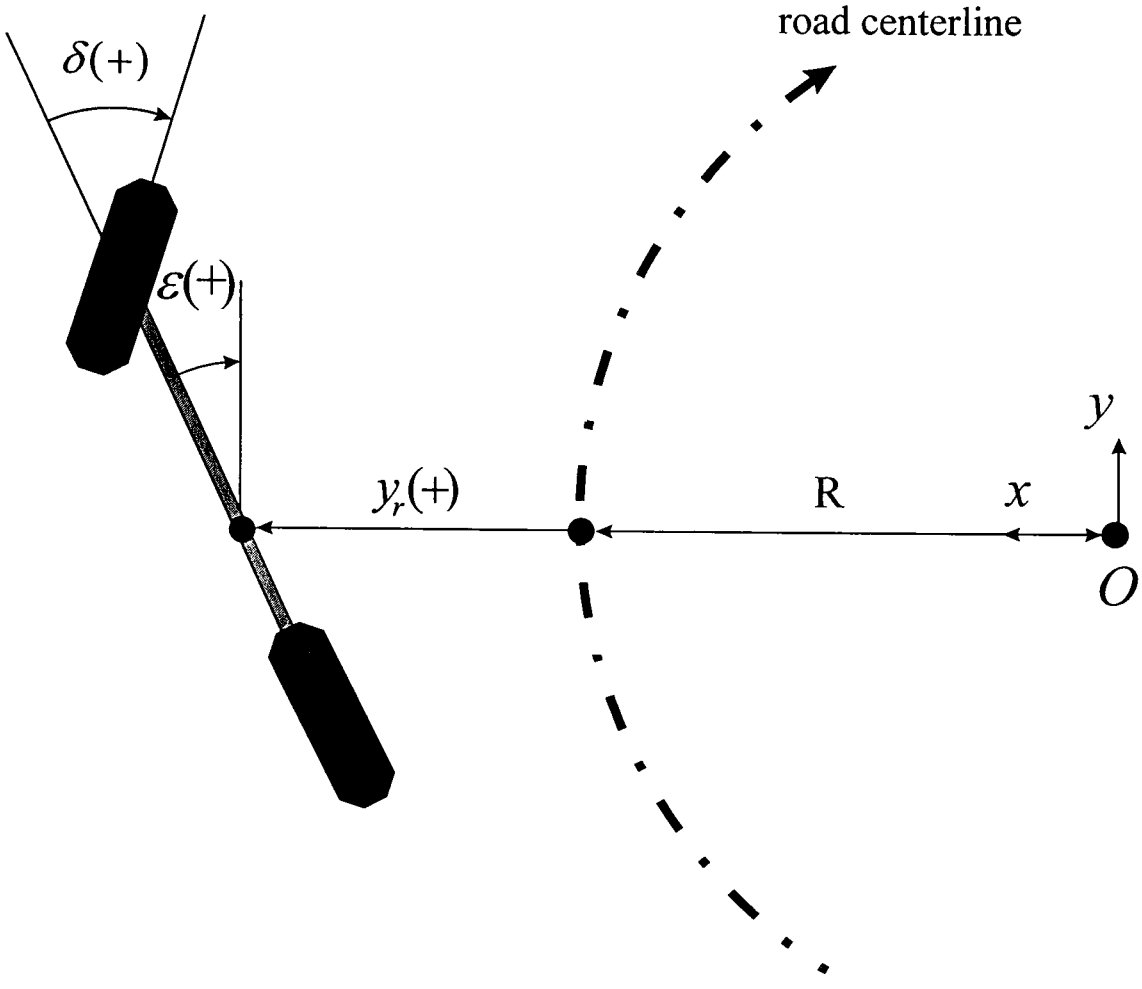

Figure 10 Coordinate system and sign conventions for right turn case.

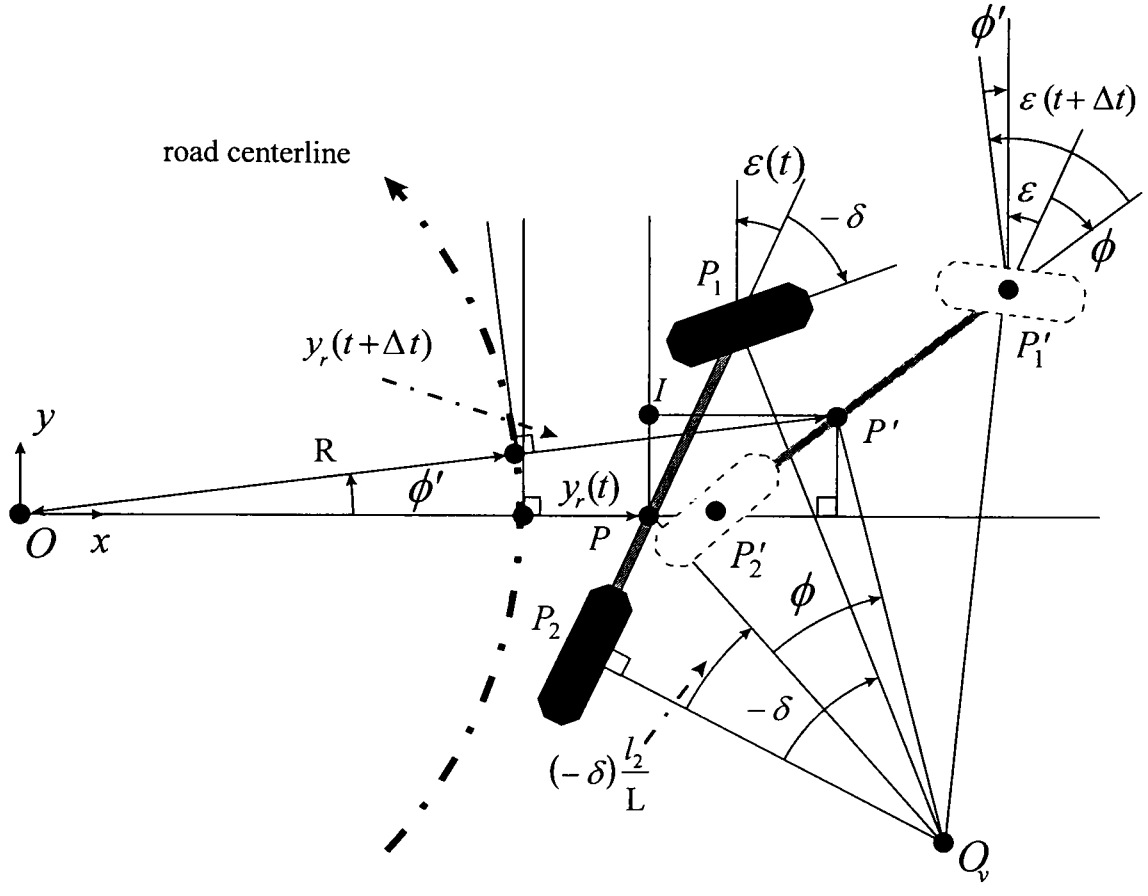

Figure 11 Problem set-up for vehicle turning to the right case (i.e. $\delta < 0$).

3.0 Simulation

Simulation Issues

The error-state Ackerman steering model derived above was simulated using MATLAB® and SIMULINK®. The simulation diagram that realizes the model was implemented in SIMULINK® , where the generic simulation diagram is presented in Fig. 12 and the actual SIMULINK® simulation diagram is given in Appendix B. The simulation parameters were selected to support the assumptions and to closely match those in the experimental setup (see Table 1). A fifth-order Runge-Kutta integrator with a minimum time step of 0.001 sec and a maximum time step of 0.01 sec (tolerance 1.0e-3) was found to work satisfactorily when generating a numerical solution to the error-state equations. Simulation results are compared directly with experimental results described below.

Table 1 Simulation Parameters

Parameters

L = 0.3 m

l_2 = 0.12 m

R = 1.92 m

r = 40 mm

V = 1.0 m / sec (not critical)

Initial Conditions (dependent on specific scenario considered)

$y_r(0)$, $\varepsilon(0)$

Input (dependent on specific scenario considered)

δ

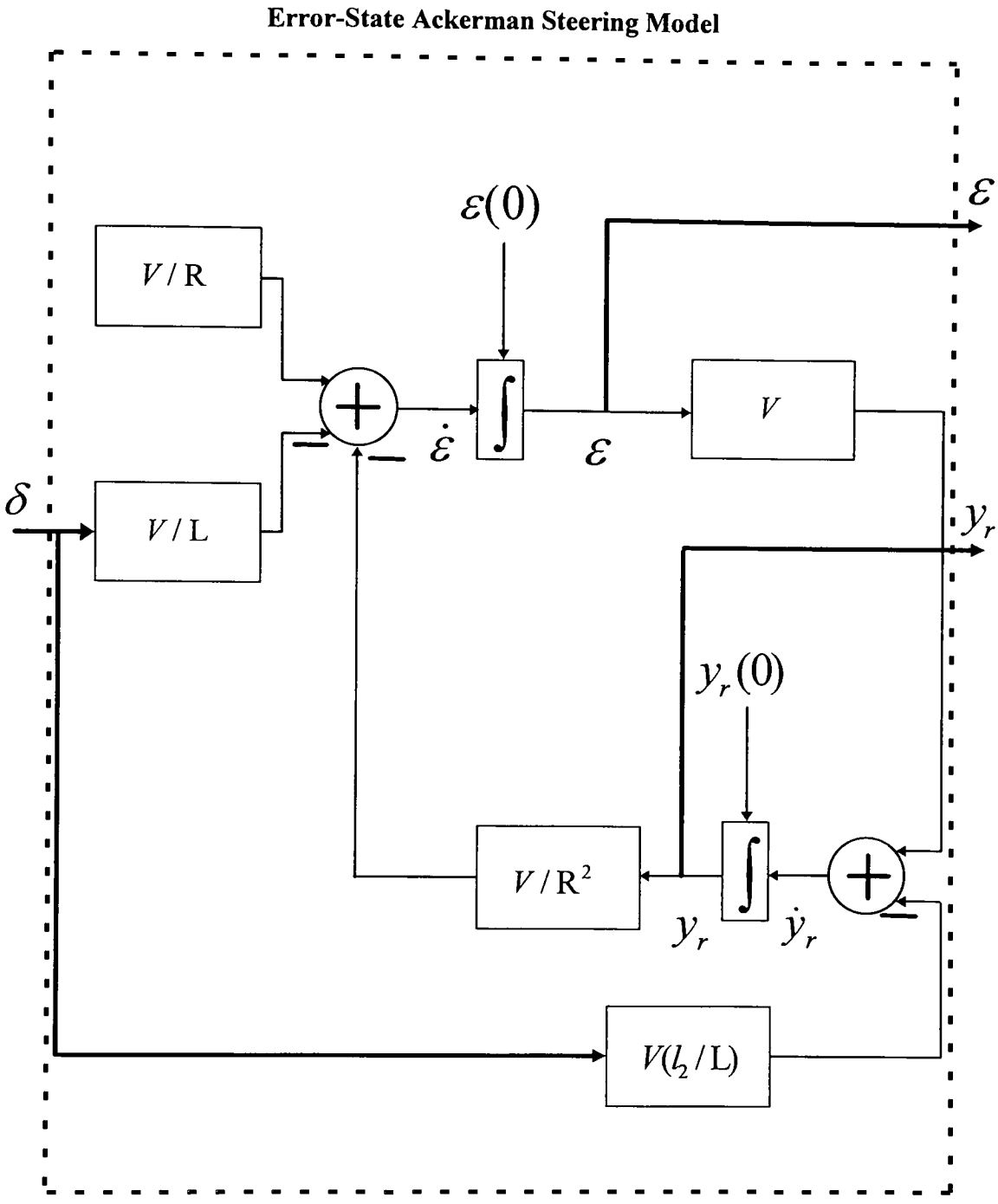

Figure 12 Simulation diagram representation of the error-state Ackerman steering model.

4.0 Experimental Results

4.1 Overview of the Experimental Set-Up and Procedure

To validate the error-state model, selective experiments were conducted using a 1 / 24 th scale model radio controlled (RC) vehicle traversing a simulated road of constant curvature (see Fig. 13)[7] . As the vehicle moves slowly, a pen mounted on-board (approximately at the CG) traces out a path on the paper road surface. In this manner different scenarios can be investigated by varying the steered wheel angle δ and the initial conditions ($y_r(0)$, $\varepsilon(0)$) appropriately, as well as the road curvature 1 / R (only parametrically). Subsequent geometrical measurements of the vehicle's path with respect to the road centerline permit a direct comparison between simulation results and experimental results.

[7] It should be noted that for these experiments the "RC" feature of the vehicle was not used. Rather, the vehicle was carefully advanced manually as the path was being generated.

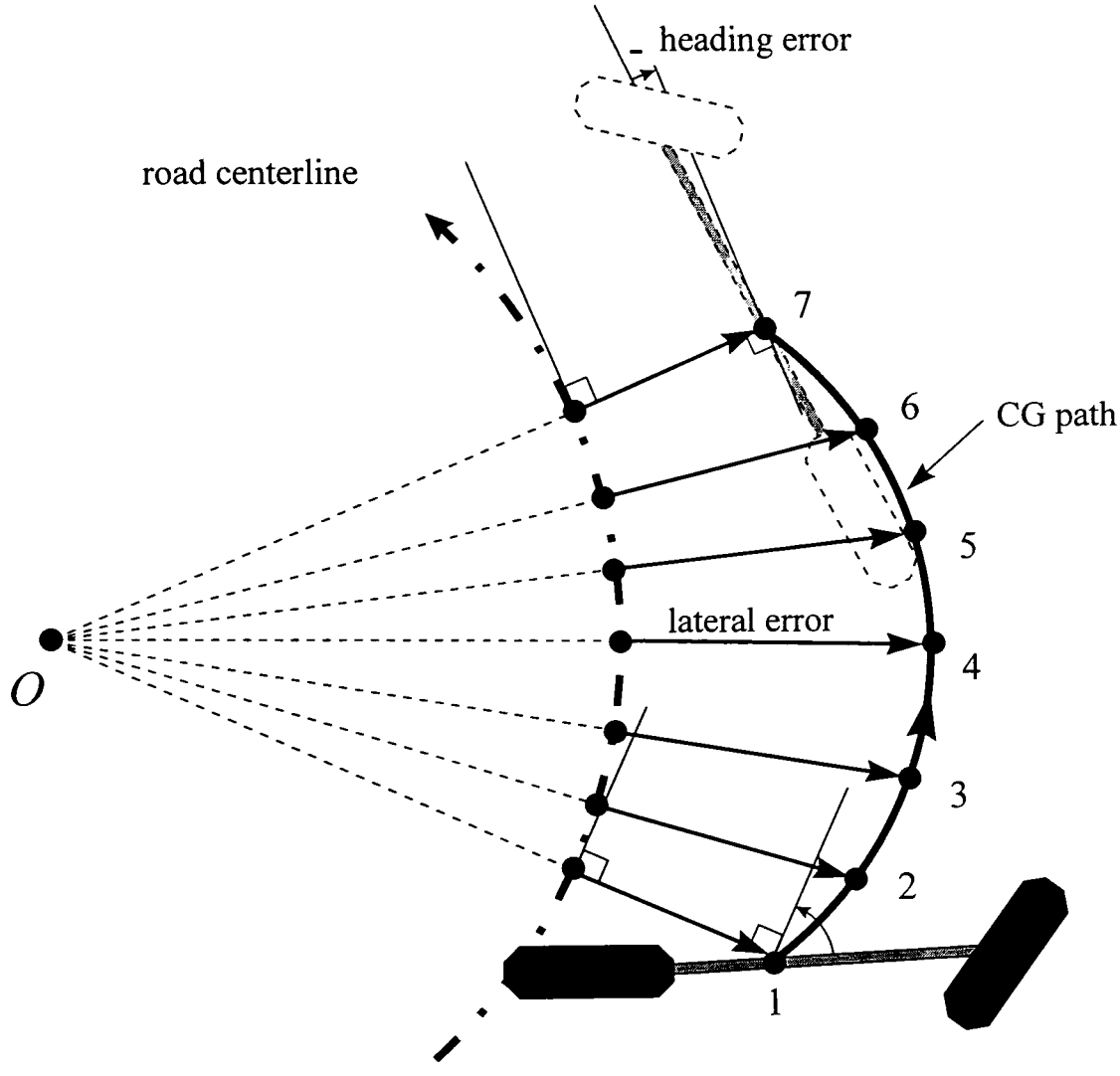

Figure 13 Experimental set-up for validation of error-state model.

4.2 Experimental Scenarios, Results, and Comparison with Simulation Results

Three different scenarios were investigated experimentally[8] :

- $\delta(t) = -12$ deg (right turn)
- $\delta(t) = 0$ deg (straight)
- $\delta(t) = 12$ deg (left turn)

In each of the above cases the initial conditions $y_r(0)$ and $\varepsilon(0)$ are assumed to be zero. As time evolved data were collected until either model linearity would clearly be violated or the vehicle moved off of the paper road surface (a significant distance). As a practical matter, violation of linearity occurred approximately when $|y_r| / R = 0.10$. The resultant CG path from the initial point to the final point was divided into 6 approximately equal portions, thereby defining 7 reference points from which the lateral error y_r and heading error ε can be determined geometrically to an accuracy of approximately ± 1 mm and ± 1 deg, respectively (see Figs. 13 and 14). With the exception of the $\delta(t) = 12$ deg scenario, interesting data were obtained and plotted for each of the cases studied (see Table 2 and Figs. 14 and 15). For the $\delta(t) = 12$ deg case the magnitude of both the lateral error and the heading error was very small for the duration of the experiment (as it should be).

[8] While time varying $\delta(t)$ scenarios are more typical in everyday driving situations, it is more difficult to obtain accurate experimental data in this instance. For this reason $\delta(t)$ was set to a constant, i.e. locked steering which can be achieved easily in practice.

To permit comparison with the error-state model, simulations were performed for each of the experimental scenarios studied above:

- Right turn
- Straight (i.e. no turn)
- Left turn

Right Turn (Straight) Scenario

Figure 14 (15) illustrates the experimental and simulation results obtained. Since time is not a variable of interest we may plot heading error ε (deg) versus lateral error y_r (mm). In general, the experimental data follows the simulation data closely over the linear range studied (± 3 deg (3 deg)) given y_r for $0 \leq y_r \leq 187$ mm (103 mm) . Also, the shape of the curve is gently convex.

Left Turn Scenario

With the front steered wheel turned to the left the vehicle will naturally veer to the left, which in this case is also the direction the road is turning. Therefore, depending on the initial conditions and the road curvature, it may be a significant time before the vehicle veers significantly off course generating nontrivial lateral and heading errors. Such was the case for both the experiment and the corresponding simulation (i.e. $\left|\varepsilon(y_r)\right| < 1$ deg for $0 \leq y_r \leq 17$ mm).

Table 2 Error-State Model Experimental Data

Data	**12 Degree Right Turn**		**12 Degree Left Turn**		**Straight (No Turn)**	
No	Lateral Error (mm)	Heading Error (deg)	Lateral Error (mm)	Heading Error (deg)	Lateral Error (mm)	Heading Error (deg)
1	0	0	0	0	0	0
2	6	4	4	0	4	3
3	19	12	8	0	12	6
4	45	17	11	0	27	10
5	81	21	14	0	47	11
6	126	27	16	0	71	13
7	187	32	17	0	103	19

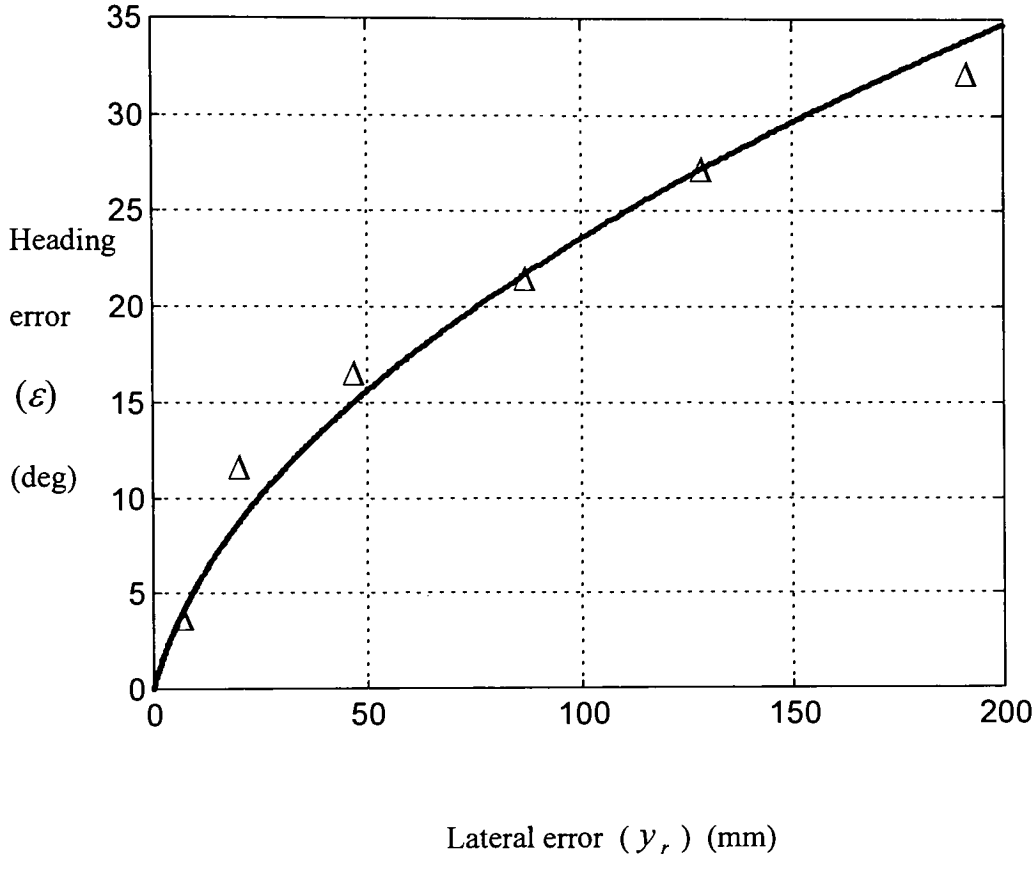

Figure 14 Experimental and simulation results when $\delta(t)$ = -12 deg (right turn), $y_r(0)$ = 0, $\varepsilon(0)$ = 0, V = 1.0 m / sec, L = 0.3 m, l_2 = 0.12 m, R = 1.92 m, and $t \in [0\ ,\ 0.519]$ (sec). Note: (Δ) represents experimental data.

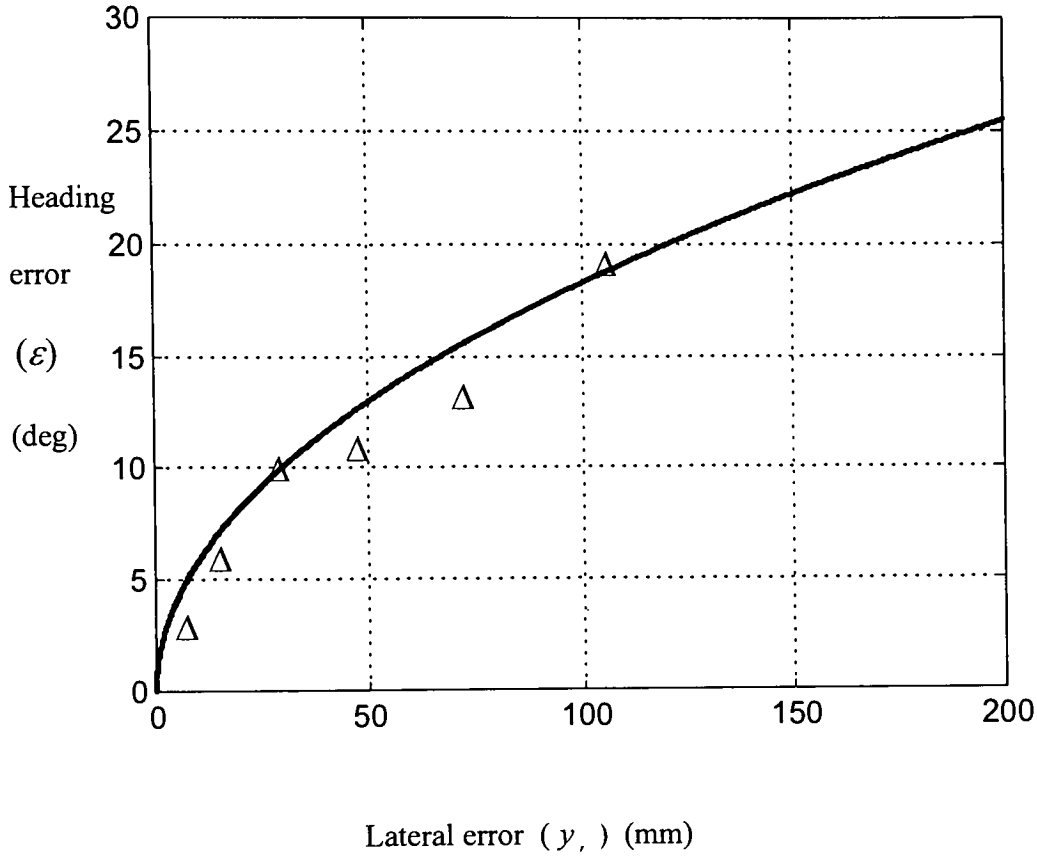

Figure 15 Experimental and simulation results when $\delta(t) = 0$ deg (straight), $y_r(0) = 0$, $\varepsilon(0) = 0$, $V = 1.0$ m / sec, L = 0.3 m, $l_2 = 0.12$ m, R = 1.92 m, and $t \in [0, 0.884]$ (sec). Note: (Δ) represents experimental data.

5.0 Conclusions

A vehicle error-state kinematic model based on Ackerman steering was derived analytically and validated through simulation and experimental work. Both linear and nonlinear models were derived. Vehicle error states considered are lateral error and heading error measured with respect to the instantaneous road centerline tangent. The significance of the "error-state" model is that it is not dependent on a global coordinate system (i.e. only local) and since the state variables are error quantities, it lends itself directly to the study of lateral guidance *control* of vehicles, of general interest to the AVCS community.

6.0 Acknowledgments

The author wishes to acknowledge the Turkish Republic's Ministry of National Education for partial support of this work.

References

1. Fenton, R. E. Melocik, G. C., and Olson, K. W., "On the Steering of Automated Vehicles: Theory and Experiment," *IEEE Trans. on Automatic Control,* Vol. AC-21, No. 3, June 1980, pp. 306-315.

2. Frankel, J., Alvarez, L., Horowitz, R., and Li, P., "Safety Oriented Maneuvers for IVHS," *Vehicle System Dynamics*, 26 (1996), pp. 271-299.

3. Hessburg, T. M., "Fuzzy Logic Control with Adaptive Methods for Vehicle Lateral Guidance," PhD. Dissertation, University of California at Berkeley, 1994.

4. Miller, G. R., "Effect of Ackerman Steering Correction Upon Front Tire Wear of Medium Duty Trucks," *SAE Technical Paper Series SAE Truck and Bus Meeting and Exposition,* 1985.

5. Miller, G. R., Reed, R., and Wheeler, F. "Optimum Ackerman for Improved Steering Axle Tire Wear on Trucks," *SAE Special Publications Commercial Vehicle Suspensions, Steering Systems, and Traction International Truck and Bus Meeting and Exposition*, n 892 November 18-21 1991, pp. 107-128.

6. O'Brien, R. T., Iglesias, P. A., and Urban, T. J., "Vehicle Lateral Control for Automated Highway Systems," *IEEE Trans. on Control Systems Technology*, Vol. 4, No. 3, May 1996.

7. Pears, N. E. and Bumby, J. R., "Guidance of an autonomous guided vehicle using low-level ultrasonic and odometry sensor systems," Trans Inst MC, Vol 11 No 5, Oct.-Dec. 1989.

8. Peng, H. and Tomizuka, M., "Preview Control for Vehicle Lateral Guidance in Highway Automation," ASME *Journal of Dynamic Systems, Measurement, and Control,* December 1993, Vol. 115, pp. 679-686.

9. Shladover, S., et al., "Steering Controller Design for Automated Guide-way Transit Vehicles," *ASME Journal of Dynamic Systems, Measurement, and Control,* Vol. 100, March 1978, pp. 1-8.

10. The MathWorks, Inc., "MATLAB® Reference Guide, High-Performance Numeric Computation and Visualization Software," Natick, MA, July 1993.

11. The MathWorks, Inc., "SIMULINK® User's Guide, Dynamic System Simulation Software, For Microsoft Windows," Natick, MA, June 1995.

12. Whitcomb, D. W. and Milliken, W. F., "Design Implications of a General Theory of Automobile Stability and Control," Engineer v 202 n 5262 Nov 30 1956 p 774-6.

13. Wong, J. Y., *Theory of Ground Vehicles.* John Wiley & Sons, Inc. 1993.

14. Young, R. E., "Highly Maneuverable Nursery Straddle Vehicle," Trans. American Society of Agricultural Engineers, v 28 n 4 Jul-Aug 1985 p 1031-1037.

15. Zang, Y. and Bigsby, F. W., "Design of Common-Center-Steering Systems of Tractors," Papers Presented at the 1986 Summer Meeting, American Society of Agricultural Engineers, 1986 San Luis Obispo, CA, USA.

Appendix A: Nonlinear Error-State Model

The abbreviated derivation presented below describes a nonlinear error-state model for the $\delta > 0$ case (refer to Figs. 1, 2, and 3). It can be shown that the resulting nonlinear equations apply to $\delta < 0$ case as well.

Preliminary Geometrical Considerations

Coordinates of point P_1 :

$$x_{P_1} = \mathrm{R} + y_r + l_1 \sin \varepsilon \tag{A-1}$$

$$y_{P_1} = l_1 \cos \varepsilon \tag{A-2}$$

Coordinates of point P_2 :

$$x_{P_2} = \mathrm{R} + y_r - l_2 \sin \varepsilon \tag{A-3}$$

$$y_{P_2} = -l_2 \cos \varepsilon \tag{A-4}$$

Coordinates of point P :

$$x_P = \mathrm{R} + y_r \tag{A-5}$$

$$y_P = 0 \tag{A-6}$$

Coordinates of point O_V :

$$\text{Slope of } \overline{O_V P_1} = \tan(\delta - \varepsilon) \tag{A-7}$$

$$\text{Slope of } \overline{O_V P_2} = -\tan \varepsilon \tag{A-8}$$

Equation of the line defined by $\overline{O_V P_1}$:

$$\frac{y - y_{P_1}}{x - x_{P_1}} = \frac{y - l_1 \cos\varepsilon}{x - \mathrm{R} - y_r - l_1 \sin\varepsilon} = \tan(\delta - \varepsilon) \tag{A-9}$$

or,

$$y = (x - \mathrm{R} - y_r - l_1 \sin\varepsilon)\tan(\delta - \varepsilon) + l_1 \cos\varepsilon \tag{A-10}$$

Equation of the line defined by $\overline{O_V P_2}$:

$$\frac{y - y_{P_2}}{x - x_{P_2}} = \frac{y + l_2 \cos\varepsilon}{x - \mathrm{R} - y_r + l_2 \sin\varepsilon} = -\tan\varepsilon \tag{A-11}$$

or,

$$y = -(x - \mathrm{R} - y_r + l_2 \sin\varepsilon)\tan\varepsilon - l_2 \cos\varepsilon \tag{A-12}$$

The coordinates of point O_V are determined by the intersection of lines $\overline{O_V P_1}$ and $\overline{O_V P_2}$:

$$\begin{aligned} y_{O_V} &= (x_{O_V} - \mathrm{R} - y_r - l_1 \sin\varepsilon)\tan(\delta - \varepsilon) + l_1 \cos\varepsilon \\ &= -(x_{O_V} - \mathrm{R} - y_r + l_2 \sin\varepsilon)\tan\varepsilon - l_2 \cos\varepsilon \end{aligned} \tag{A-13}$$

Solving Eq. (A-13) for x_{O_V} yields:

$$x_{O_V} = \mathrm{R} + y_r + \frac{1}{\tan(\delta - \varepsilon) + \tan\varepsilon}\left[l_1 \sin\varepsilon\left(\tan(\delta - \varepsilon) - \frac{1}{\tan\varepsilon}\right) - l_2 \frac{1}{\cos\varepsilon}\right] \tag{A-14}$$

Substitution of x_{O_V} into Eq. (A-13) yields:

$$y_{O_V} = -\frac{1}{\tan(\delta - \varepsilon) + \tan\varepsilon}\left[l_1 \tan\varepsilon \sin\varepsilon\left(\tan(\delta - \varepsilon) - \frac{1}{\tan\varepsilon}\right) + l_2 \frac{\tan(\delta - \varepsilon)}{\cos\varepsilon}\right] \tag{A-15}$$

Coordinates of point P':

The coordinates of point P' may be determined by rotating point P an angle ϕ about point O_V:

$$\begin{bmatrix} x_{P'} \\ y_{P'} \end{bmatrix} = \begin{bmatrix} x_{O_V} \\ y_{O_V} \end{bmatrix} + \begin{bmatrix} \cos\phi & -\sin\phi \\ \sin\phi & \cos\phi \end{bmatrix} \begin{bmatrix} (\mathrm{R}+y_r)-x_{O_V} \\ 0-y_{O_V} \end{bmatrix} \tag{A-16}$$

Since ϕ is proportional to Δt, and Δt is small:

$$\begin{bmatrix} x_{P'} \\ y_{P'} \end{bmatrix} \cong \begin{bmatrix} x_{O_V} \\ y_{O_V} \end{bmatrix} + \begin{bmatrix} 1 & -\phi \\ \phi & 1 \end{bmatrix} \begin{bmatrix} (\mathrm{R}+y_r)-x_{O_V} \\ -y_{O_V} \end{bmatrix} \tag{A-17}$$

or, in scalar form:

$$x_{P'} = x_{O_V} + \mathrm{R} + y_r - x_{O_V} + \phi y_{O_V} = \mathrm{R} + y_r + \phi y_{O_V} \tag{A-18}$$

$$y_{P'} = y_{O_V} + \phi(\mathrm{R} + y_r - x_{O_V}) - y_{O_V} = \phi(\mathrm{R} + y_r - x_{O_V}) \tag{A-19}$$

Substitution of x_{O_V} and y_{O_V} from Eqs. (A-14) and (A-15), respectively, into Eqs. (A-18) and (A-19) will give us the coordinates of point P':

$$\begin{aligned} x_{P'} = \mathrm{R} + y_r - \frac{\phi}{\tan(\delta-\varepsilon)+\tan\varepsilon} \times \\ \left[l_1 \tan\varepsilon \sin\varepsilon \left(\tan(\delta-\varepsilon) - \frac{1}{\tan\varepsilon} \right) + l_2 \frac{\tan(\delta-\varepsilon)}{\cos\varepsilon} \right] \end{aligned} \tag{A-20}$$

$$y_{P'} = -\frac{\phi}{\tan(\delta-\varepsilon)+\tan\varepsilon} \left[l_1 \sin\varepsilon \left(\tan(\delta-\varepsilon) - \frac{1}{\tan\varepsilon} \right) - l_2 \frac{1}{\cos\varepsilon} \right] \tag{A-21}$$

$|\overline{OP'}|$:

$|\overline{OP'}|$ can be derived by the Pythagorean theorem as follows:

$$|\overline{OP'}|^2 = x_{P'}{}^2 + y_{P'}{}^2 = (\mathrm{R}+y_r)^2 - 2(\mathrm{R}+y_r)\frac{\phi}{\tan(\delta-\varepsilon)+\tan\varepsilon}\times \\ \left[\ l_1 \tan\varepsilon\sin\varepsilon\left(\tan(\delta-\varepsilon)-\frac{1}{\tan\varepsilon}\right)+l_2\frac{\tan(\delta-\varepsilon)}{\cos\varepsilon}\ \right] \tag{A-22}$$

where the ϕ^2 term has been ignored since $\phi \propto \Delta t$ and $\Delta t \to 0$. In particular, ϕ is parameterized as $\phi = \frac{V}{\mathrm{R}_{P_2}}\Delta t$ where V is chosen to be the longitudinal velocity of point P_2 (i.e. speed at rear wheel) and R_{P_2} is the radius of curvature measured at point P_2.

Substitution of ϕ into the above equation gives:

$$x_{P'}{}^2 + y_{P'}{}^2 = (\mathrm{R}+y_r)^2 - 2(\mathrm{R}+y_r)\frac{V\Delta t}{\mathrm{R}_{P_2}\left[\tan(\delta-\varepsilon)+\tan\varepsilon\right]}\times \\ \left[\ l_1 \tan\varepsilon\sin\varepsilon\left(\tan(\delta-\varepsilon)-\frac{1}{\tan\varepsilon}\right)+l_2\frac{\tan(\delta-\varepsilon)}{\cos\varepsilon}\ \right] \tag{A-23}$$

The structure of Eq. (A-23) is such that it has a simple Taylor series expansion in Δt :

$$|OP'| = (x_{P'}{}^2 + y_{P'}{}^2)^{1/2} \equiv (\mathrm{A}+\mathrm{B}\Delta t)^{1/2} = \mathrm{A}^{1/2}\left(\ 1+\frac{\mathrm{B}}{\mathrm{A}}\Delta t\ \right)^{1/2} \cong \mathrm{A}^{1/2}\left(\ 1+\frac{\mathrm{B}}{2\mathrm{A}}\Delta t\ \right) \tag{A-24}$$

where A and B are defined appropriately, i.e.:

$$\mathrm{A} = (\mathrm{R}+y_r)^2 \tag{A-25}$$

$$\mathrm{B} = -2(\mathrm{R}+y_r)\frac{V}{\mathrm{R}_{P_2}\left[\tan(\delta-\varepsilon)+\tan\varepsilon\right]}\times$$
$$\left[\; l_1\tan\varepsilon\sin\varepsilon\left(\tan(\delta-\varepsilon)-\frac{1}{\tan\varepsilon}\right)+l_2\frac{\tan(\delta-\varepsilon)}{\cos\varepsilon}\;\right] \tag{A-26}$$

Thus,

$$|OP'| \cong (R+y_r)(1+\frac{B}{2A}\Delta t) \tag{A-27}$$

Lateral Error State Equation:

The lateral error at time $t+\Delta t$ is given by:

$$y_r(t+\Delta t) = (\mathrm{R}+y_r)(1+\frac{\mathrm{B}}{2\mathrm{A}}\Delta t)-\mathrm{R} \tag{A-28}$$

We may now evaluate the time derivative of the lateral error:

$$\dot{y}_r = \lim_{\Delta t\to 0}\frac{y_r(t+\Delta t)-y_r(t)}{\Delta t} \tag{A-29}$$

From Eqs. (A-28) and (A-29) it follows that:

$$\dot{y}_r = -\frac{V}{\mathrm{R}_{P_2}\left[\tan(\delta-\varepsilon)+\tan\varepsilon\right]}\times$$
$$\left[\; l_1\tan\varepsilon\sin\varepsilon\left(\tan(\delta-\varepsilon)-\frac{1}{\tan\varepsilon}\right)+l_2\frac{\tan(\delta-\varepsilon)}{\cos\varepsilon}\;\right] \tag{A-30}$$

Finally, substitution of $\mathrm{R}_{P_2} = \dfrac{\mathrm{L}}{\tan\delta}$ into Eq. (A-30) gives us the nonlinear lateral error-state equation:

$$\boxed{\dot{y}_r = -\frac{V\tan\delta}{\mathrm{L}\left[\tan(\delta-\varepsilon)+\tan\varepsilon\right]}\times \left[\; l_1\tan\varepsilon\sin\varepsilon\left(\tan(\delta-\varepsilon)-\frac{1}{\tan\varepsilon}\right)+l_2\frac{\tan(\delta-\varepsilon)}{\cos\varepsilon}\;\right]} \tag{A-31}$$

Also, it may be easily shown that the above equation when linearized, agrees with the previously derived linear model (Eq. (23)).

Heading Error State Equation:

Since by assumption ϕ' is sufficiently small so the trigonometric nonlinearity may be ignored,

$$\phi' \cong \tan\phi' = \frac{y_{P'}}{x_{P'}} \tag{A-32}$$

Therefore:

$$\phi' \cong \frac{\phi \mathrm{D}}{\mathrm{R} + y_r + \phi \mathrm{C}} \tag{A-33}$$

where,

$$\mathrm{C} = -\frac{1}{\tan(\delta-\varepsilon)+\tan\varepsilon}\Big[\, l_1 \tan\varepsilon \sin\varepsilon \times \left(\tan(\delta-\varepsilon) - \frac{1}{\tan\varepsilon}\right) + l_2 \frac{\tan(\delta-\varepsilon)}{\cos\varepsilon} \,\Big] \tag{A-34}$$

$$\mathrm{D} = -\frac{1}{\tan(\delta-\varepsilon)+\tan\varepsilon} \times \Big[\, l_1 \sin\varepsilon \left(\tan(\delta-\varepsilon) - \frac{1}{\tan\varepsilon}\right) - l_2 \frac{1}{\cos\varepsilon} \,\Big] \tag{A-35}$$

As in the lateral error state equation derivation, the heading error $\Delta\varepsilon$ is:

$$\Delta\varepsilon = \varepsilon(t+\Delta t) - \varepsilon(t) = \phi' - \phi \tag{A-36}$$

$$\Delta\varepsilon \cong \frac{\phi \mathrm{D} - \mathrm{R}\phi - y_r\phi - \phi^2 \mathrm{C}}{\mathrm{R} + y_r + \phi \mathrm{C}} \tag{A-37}$$

If the ϕ^2 term is neglected then Eq. (A-37) reduces to:

$$\Delta\varepsilon = \frac{\phi\,\mathrm{D} - \mathrm{R}\phi - y_r\phi}{\mathrm{R} + y_r + \phi\,\mathrm{C}} \tag{A-38}$$

From the above expression we may evaluate the time derivative of ε as follows:

$$\dot{\varepsilon} = \frac{V\tan\delta\,\left(\,\mathrm{D} - \mathrm{R} - y_r\,\right)}{\mathrm{L}\,(\mathrm{R} + y_r)} \tag{A-39}$$

or after substitution,

$$\dot{\varepsilon} = \frac{V\tan\delta}{\mathrm{L}}\left\{\frac{1}{\mathrm{R}+y_r}\left[-\frac{1}{\tan(\delta-\varepsilon)+\tan\varepsilon}\times \left[\, l_1\sin\varepsilon\left(\tan(\delta-\varepsilon)-\frac{1}{\tan\varepsilon}\right) - l_2\frac{1}{\cos\varepsilon}\,\right]\right] - 1\right\} \tag{A-40}$$

Also, it may be easily shown that the above equation when linearized agrees with the previously derived linear model (Eq. (32)).

Appendix B SIMULINK® Simulation Diagram

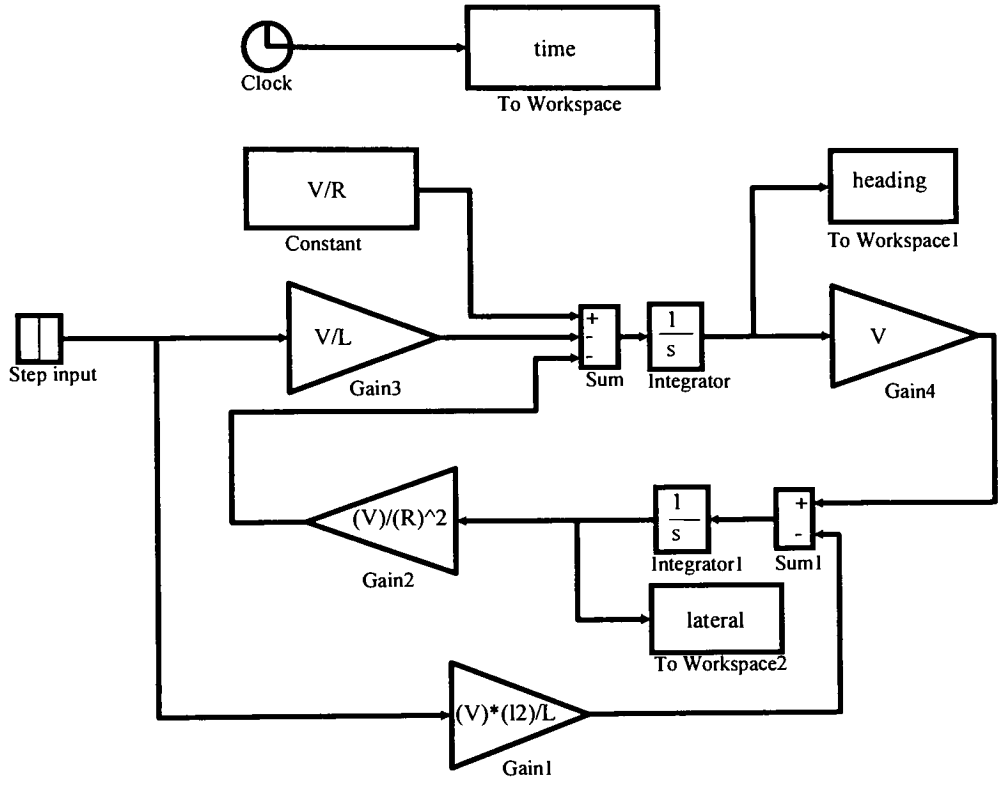

Lateral Guidance Control of a Low-Speed Vehicle Using Fuzzy Logic

by

Haydar Sahin
Department of Mechanical Engineering
College of Engineering
Rochester Institute of Technology
Rochester, New York
August 1997

ABSTRACT

This paper investigates the performance of several different controllers used to perform lateral guidance control of a low-speed vehicle described by a linear nonminimum-phase "error-state" bicycle model based on Ackerman steering. Both a conventional type I proportional-integral (PI) controller and a fuzzy logic controller (FLC) are considered. The PI controller is designed using standard techniques and the two-level FLC / PI controller adjusts both proportional and integral feedback control gains around the baseline values based on heuristics and the current conditions as measured by the lateral error. Time-based simulations using MATLAB® / SIMULINK® permit a comparison between both controllers for several different simulation scenarios of interest. Primary performance metrics considered were settling time and percent overshoot in response to a step input. In general, the two-level FLC / PI controller performed better; 6 % reduction in overshoot and 21 % reduction in settling time.

Lateral Guidance Control of a Low-Speed Vehicle Using Fuzzy Logic

TABLE OF CONTENTS

NOMENCLATURE

POINTS IN SPACE

O	Point representing the center of road curvature
O_v	Point representing the center of vehicle's curvature based on Ackerman steering model
P	Point representing the vehicle's center of gravity (CG) at time t
P_1	Point representing the center of the front wheel at time t
P_2	Point representing the center of the rear wheel at time t

CONSTANTS OR PARAMETERS

e	Lateral error from command [m]
e_{ss}	Steady - state lateral error [m]
γ	Phase margin [deg]
j	$\sqrt{-1}$ [unitless]
K_d	Derivative feedback gain [rad · sec / m]
K_g	Gain margin [dB]
K_i	Integral feedback gain [rad / m · sec]
K_p	Proportional feedback gain [rad / m]
L	Distance between axles: $l_1 + l_2$ [m]
l_1	Distance from CG to the front axle [m]
l_2	Distance from CG to the rear axle [m]
M_p	Percent overshoot [%]
R	Radius of road centerline curvature [m]
r	Radius of tires [m]
t_s	Settling time [sec]
V	Longitudinal vehicle speed [m / sec]
y_{rc}	Lateral error step input command [m]

VARIABLES & FUNCTIONS

δ	Front wheel steering angle [deg or rad]
e(t)	Error signal: $y_{rc} - y_r$ [m]
$\varepsilon(t)$	Vehicle heading error at time t [deg or rad]
s	Laplace variable [rad / sec]
t	Time [sec]
U(t)	Unit step function [unitless]
ω	Angular frequency [rad / sec]
$y_r(t)$	Lateral error at time t [m]

TRANSFER FUNCTIONS & LAPLACE DOMAIN FUNCTIONS

D(s)	Laplace transform of road curvature disturbance
Δ(s)	Laplace transform of steered wheel angle $\delta(t)$
E(s)	Laplace transform of error signal, e(t)
G(s)	Loop gain transfer function: $G_c(s)G_p(s)$
$G_c(s)$	Transfer function of controller
$G_p(s)$	Transfer function of plant
$Y_r(s)$	Laplace transform of lateral error, y_r
$Y_{rc}(s)$	Laplace transform of lateral error command, y_{rc}

FUZZY LOGIC CONTROL (FLC) NOTATION

TERMINOLOGY	ABBREVIATION
Lateral error	LE
Negative	NEG
Positive	POS
Zero	ZERO

1.0 Introduction

Background

Considerable research is underway to automatically control vehicles in order to increase highway throughput or to assist drivers in certain critical safety situations. Much of this work falls under the umbrella of what is referred to as the Autonomous Highway System (AHS) Program and / or the Intelligent Transportation System (ITS) (formerly known as the Intelligent Vehicle Highway System (IVHS)) Program. ITS is divided into two categories which are further sub-divided into a total of six divisions. The first category is technology oriented and is concerned with Advanced Traffic Management Systems (ATMS), Advanced Traveler Information Systems (ATIS), and Advanced Vehicle Control Systems (AVCS). The second category is application oriented and includes Advanced Public Transportation Systems (APTS), Commercial Vehicle Operations (CVO), Advanced Rural Transportation Systems (ARTS), among other areas. In general, advanced technologies applied to ITS have the potential to undo damage caused by past transportation policies by improving air quality, reducing traffic congestion, and minimizing energy use and accidents.

A key component of ITS technology concerns the advanced vehicle control system (AVCS) to be used by each vehicle. In fact, throughout the whole spectrum of ITS, it is perhaps the most technically challenging and costly endeavor. AVCS in turn includes four different areas: (1) Collision Avoidance, (2) Control and Guidance, (3) Communication Systems, and (4) Intermediate Products. Control and Guidance is

divided into two parts: lateral control and longitudinal control (e.g. as described in Frankel et al. (1996)). Lateral guidance control offers opportunities for congestion relief, fuel conservation, reduction in traffic related deaths and injuries, and environmental protection.

A number of organizations throughout the US are actively involved in ITS / AVCS related research. Research is being conducted on the instrumentation of vehicles (e.g. at Virginia Polytechnic University, University of Michigan Transportation Research Institute (UMTRI)) and through use of elaborate simulation software (e.g. NAVLAB at Carnegie Mellon University, and UMTRI). Since it is less expensive to simulate highway systems rather than to build them, precise simulation systems will help researchers examine their systems in a virtual environment. One of the most important and challenging AVCS research problems concerns the development of intelligent control algorithms (e.g. fuzzy logic, neural networks, genetic algorithms, fuzzy model reference learning control). Partners for Advanced Transportation and Highways (PATH), affiliated with the University of California at Berkeley, Ohio State University and the University of Minnesota are examples of organizations actively researching intelligent control algorithms for AVCS.

Research Problem Statement

Today, perhaps PATH has the most advanced research ongoing in the area of lateral guidance control of vehicles, especially for highway applications. At PATH, Peng and Tomizuka (1993) have developed *preview control* for lateral guidance control of

vehicles in highway automation. Hessburg (1994) has successfully applied fuzzy logic, fuzzy model reference learning control, and genetic algorithms to lateral guidance control of a vehicle. Research has been both of a theoretical nature and an experimental nature, applying the algorithms to full-sized test vehicles operating on test tracks where possible.

In both of the above cases the intent is to control vehicles moving at highway speeds, typically 100+ KPH. Although vehicles driving at low speeds are commonplace in rural and urban settings (e.g. streets and parking lots), there has been very little research on lateral guidance control of low-speed vehicles. Clearly, in order to achieve higher speeds, such as on the highway, lower speeds need to be achieved first. Also, restrictions on locations for highways and their high cost makes low-speed controlled vehicles inevitable. Control of low-speed vehicles will integrate highways with rural and urban area roads which will make AVCS possible to some level on all roads. Therefore, as a practical matter, it is not possible to neglect the control of low-speed vehicles. While some autonomous guided vehicle (AGV) related research is relevant, as in Pears and Bumby (1989) where imaginary-line following is considered, more research is needed in the area of *lateral guidance control of low-speed vehicles*, especially for non-holonomic[1] vehicles such as typical cars and trucks.

[1] Non-holonomic, versus holonomic or omni-directional vehicles, for which there is a large body of research, especially regarding control of robotic vehicles in somewhat unstructured low-speed settings. Also, in a non-holonomic vehicle system there are certain directions in which the vehicle can not move without wheel slippage, i.e. sideways.

Below a baseline lateral guidance controller using classical control (i.e. proportional-integral (PI)) is developed and compared to a controller based on use of fuzzy logic. Fuzzy logic control was selected based in part on the success of Hessburg's work [1994] for the case of high speed vehicles. Also, the fuzzy logic controller developed incorporates the baseline PI controller in the sense that the low-level structure of the controller is of the "PI" type and the gain ranges considered overlap those used in the baseline controller case. To aid in the development of the controllers and to permit the simulation of their performance a vehicle model is needed. The vehicle model used is characterized as a linear error-state bicycle model (see Fig. 1) based on Ackerman steering; previously developed by Sahin (1997):

Lateral Error State Equation:

$$\dot{y}_r = V\varepsilon - \frac{l_2}{L} V\delta \tag{1}$$

Heading Error State Equation:

$$\dot{\varepsilon} = -V\frac{y_r}{R^2} - V\frac{\delta}{L} + \frac{V}{R} \tag{2}$$

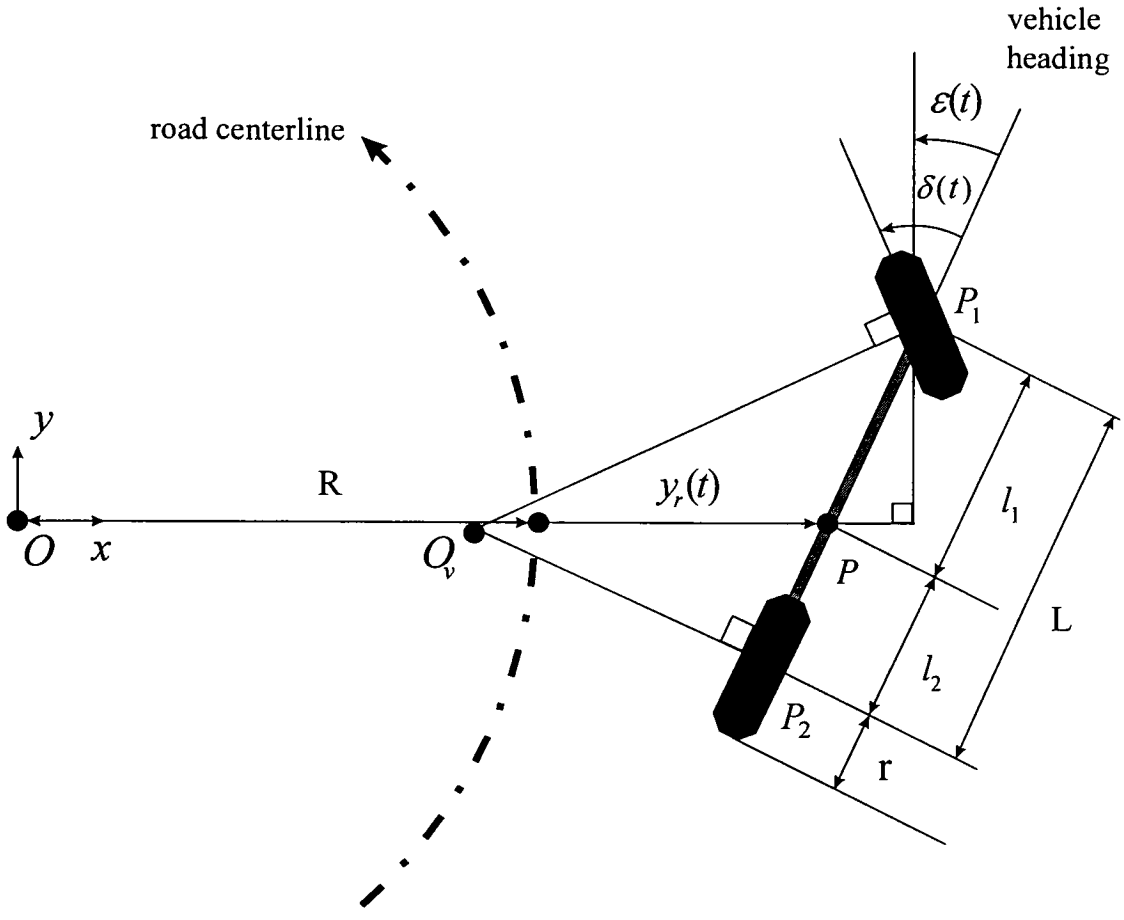

Figure 1 Error-state bicycle model based on Ackerman steering.

2.0 Baseline PI Controller

A proportional-integral (PI) controller based on measurement of lateral error was designed to serve as a baseline controller that other controllers can be compared to, such as a fuzzy logic controller. A PI controller was selected because it offers a reasonable compromise between simplicity and performance for the case of small lateral and heading errors. Below, key features of the baseline PI controller design are discussed in detail such as: problem set-up, controller design criteria, root locus, Nyquist plot, step response, bandwidth, and steady-state error when tracking a step input.

Problem Set-Up: To apply the classical control design methodology a transfer function representation for both the controller (G_c (s)) and the plant (G_p (s)) must be used and a block diagram (i.e. in the Laplace domain) constructed as shown in Fig. 2. Initial conditions for y_r and ε must be zero and unity feedback assumed as shown. The input to the controller $Y_{rc}(s)$ is a lateral error command measured from the road centerline, the output of the controller G_c (s) is the steered wheel angle $\Delta(s)$, the plant output is the lateral error ($Y_r(s)$ without the disturbance added), D(s) is the road curvature disturbance, and E(s) is the error signal (command lateral error minus actual lateral error). For the plant under consideration, and the type of control used (PI), it may be shown with the aid of Eqs. (1) - (2) that G_c (s), G_p (s), and D(s) are given by (see Appendix A):

$$G_c(s) = \frac{(K_p s + K_i)}{s} \equiv \frac{-K_p\left(s + \frac{K_i}{K_p}\right)}{s}, \text{ with } K_p,\ K_i > 0 \qquad (3)$$

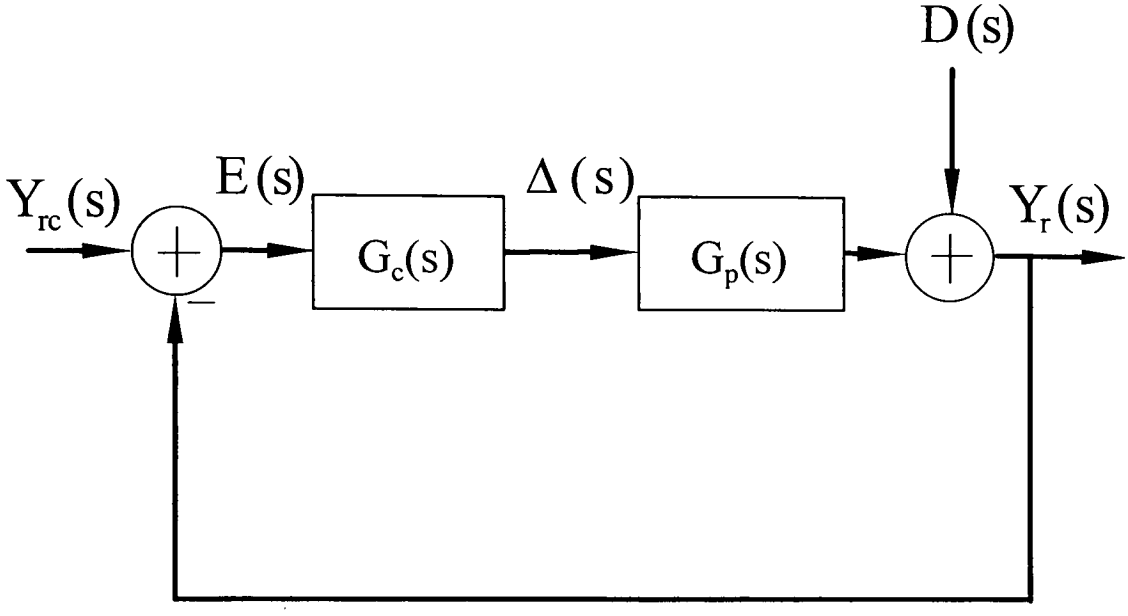

Figure 2 Baseline controller set-up in standard form.

$$G_p(s) = \frac{-\left(\frac{Vl_2}{L}\right)\left(s + \frac{V}{l_2}\right)}{s^2 + \frac{V^2}{R^2}} \tag{4}$$

$$D(s) = \frac{\frac{V^2}{R}}{s\left(s^2 + \frac{V^2}{R^2}\right)} \tag{5}$$

For convenience in the design of the controller we may elect to ignore the minus signs in both $G_c(s)$ and $G_p(s)$ since they effectively cancel each other. However, when the controller is implemented the minus sign must be retained (i.e. the actual controller gains will be negative). Note that because of the presence of the $j\omega$-axis poles in $G_p(s)$, the plant $G_p(s)$ is considered to be nonminimum-phase (Kuo (1995)). This comment also applies to the loop gain transfer function (or system) $G(s) = G_c(s)G_p(s)$, which has three poles and two zeros.

Controller Design Criteria: It is desired that a PI controller be designed such that the closed-loop system satisfies the following criteria:

- Gain margin > 6 dB (as suggested by Ogata, 1997)
- Phase margin 30-60 deg (as suggested by Ogata, 1997)
- Step response (1 mm step input) parameters:
  - zero steady-state error
  - < 30 % overshoot
  - realistic controller output (plant input)

Root Locus: A root locus plot for the system G(s) (i.e. ignoring the disturbance D(s)) is shown in Fig. 3. There are only two stable "configurations" possible: compensator zero to the left (or to the right and left of the origin) of the plant zero. We have shown the preferred configuration (compensator zero to the right of plant zero and to the left of the origin), otherwise $|\delta(t)|$ can be too large so as not to be realistic, e.g. a significant overshoot exists due to the large integral feedback gain K_i. On the other hand, if the compensator zero is placed too close to the origin, the settling time and steady-state error are compromised unnecessarily. Given the nominal plant parameters $V = 0.5$ m / sec, R = 10 m, $l_2 = 0.12$ m, and L = 0.30 m, the closed-loop poles for the controller designed are shown and correspond to a "gain margin" K_g = 19 dB (≈ 9). Since the system G(s) is nonminimum-phase, the gain margin in this context refers to the existing positive multiplicative factor above the gain required to stabilize the system[2] As can be seen from the root locus plot, with insufficient loop gain the closed-loop system will not be stable. To summarize, the controller design is: $K_p = 30$ rad / m, $K_i = 24$ rad / m $\cdot$ sec.

Nyquist Plot: The polar, or Nyquist plot of G(s) is shown in Fig. 4. From this plot both the gain margin K_g and phase margin γ can be determined graphically. For the controller selected the gain margin K_g = 19 dB (above the 6 dB lower bound) and the phase margin $\gamma = 57$ deg, (within the desirable range of 30-60 deg).

[2] Note: this definition of gain margin is different from the usual definition of gain margin for *minimum-phase* systems.

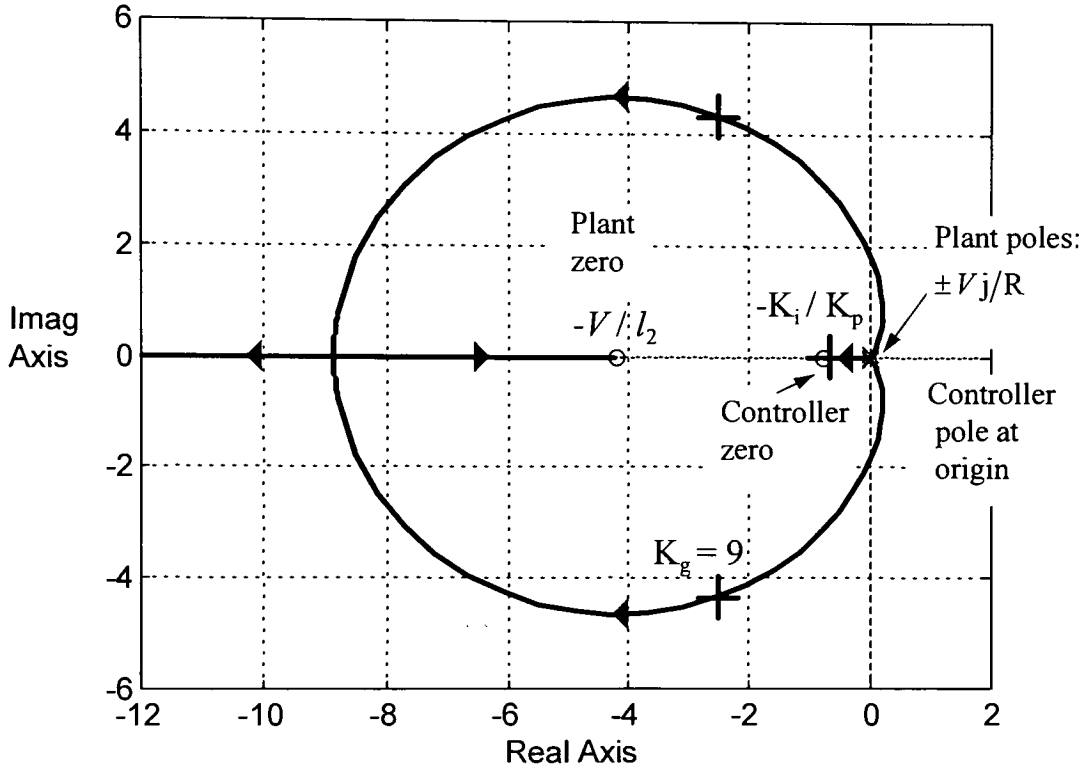

Figure 3 Root locus plot of G(s) and illustration of closed-loop poles (with "+"), $K_p = 30$ rad / m, $K_i = 24$ rad / m · sec.

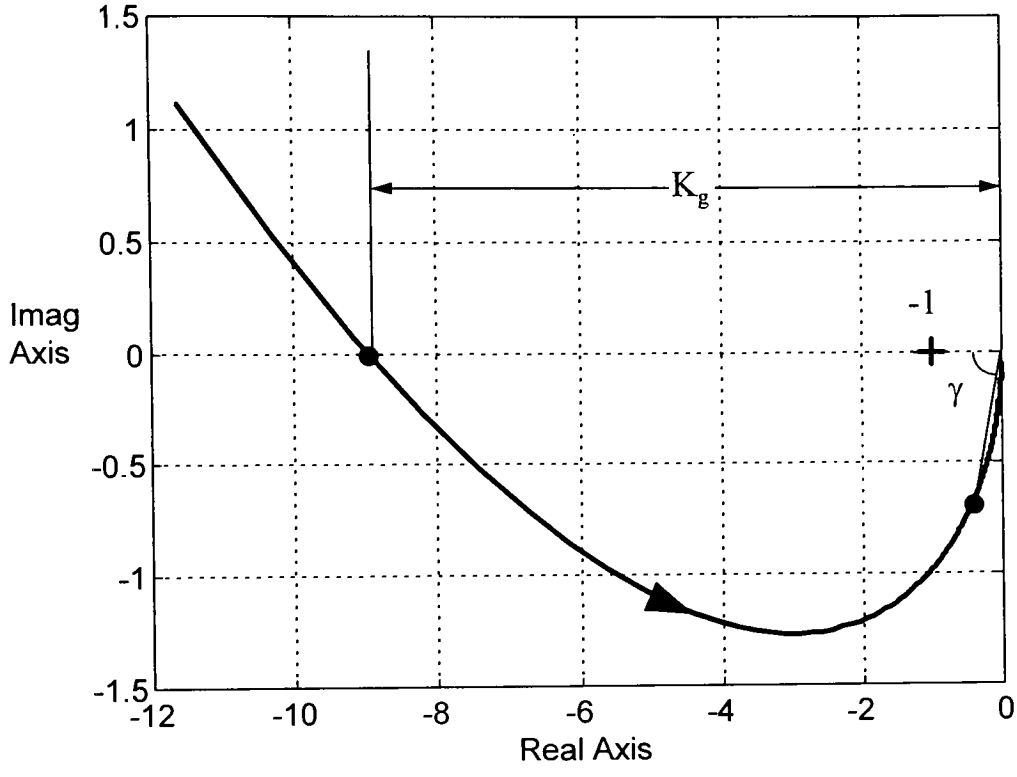

Figure 4 Polar (Nyquist) plot of G(s) ($\omega \in [2.7 , 100]$ rad / sec).

Step Response: Key to the closed-loop system's performance is its step response as shown in Fig. 5 for a step input command of y_{rc} = U(t) mm. The settling time t_s = 1.4 sec (5% criterion) and the overshoot M_p = 30 %. Of practical interest is $|\delta(t)|$. It must be realistic, e.g. not too large. By analogy to life size vehicles, a value of max$|\delta|$ in the small single digit degree range would appear to be reasonable for typical small maneuvers, such as those being simulated. For the baseline controller, and the step response considered, max $|\delta|$ = 1.8 deg.

Bandwidth: From Fig. 6 the bandwidth of the closed-loop system is 1.75 Hz (-3 dB criterion), although 0.5 Hz is perhaps more realistic since there is a significant phase lag at 1.75 Hz. Also, the cutoff rate is a modest -20 dB / decade as expected based on the nature of the controller & plant.

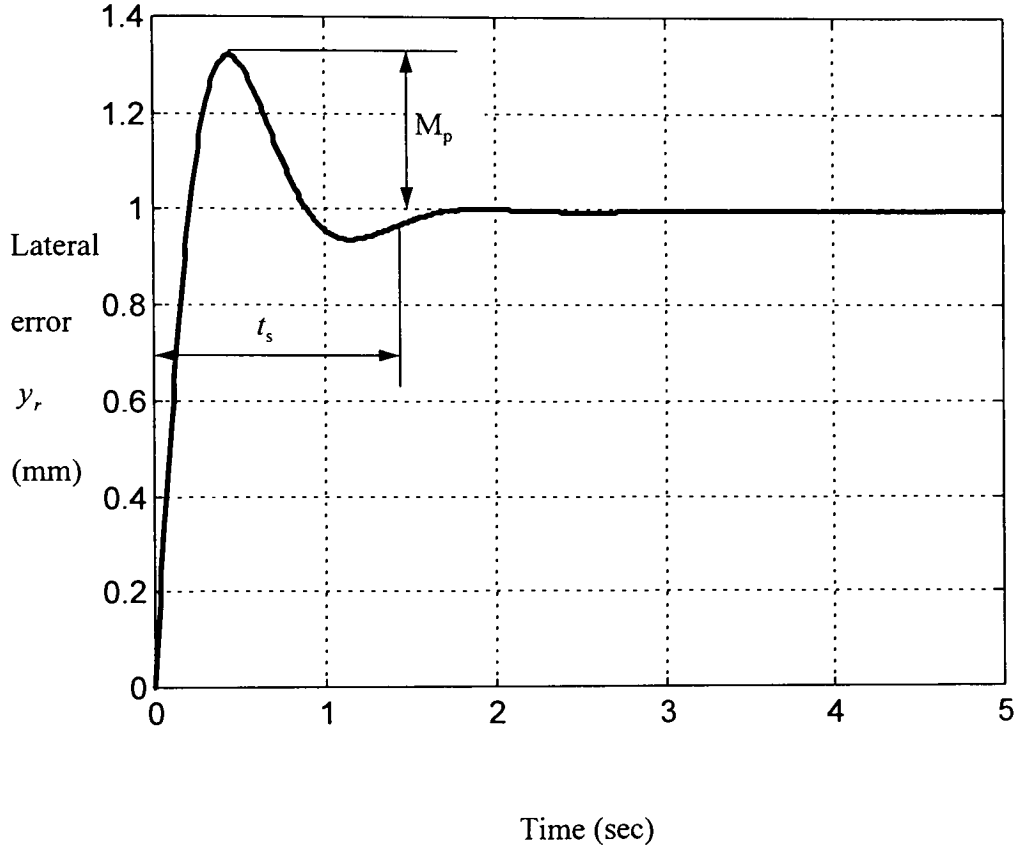

Figure 5 Step response of system for selected controller, $y_{rc}(t) = \mathrm{U}(t)$ [mm].

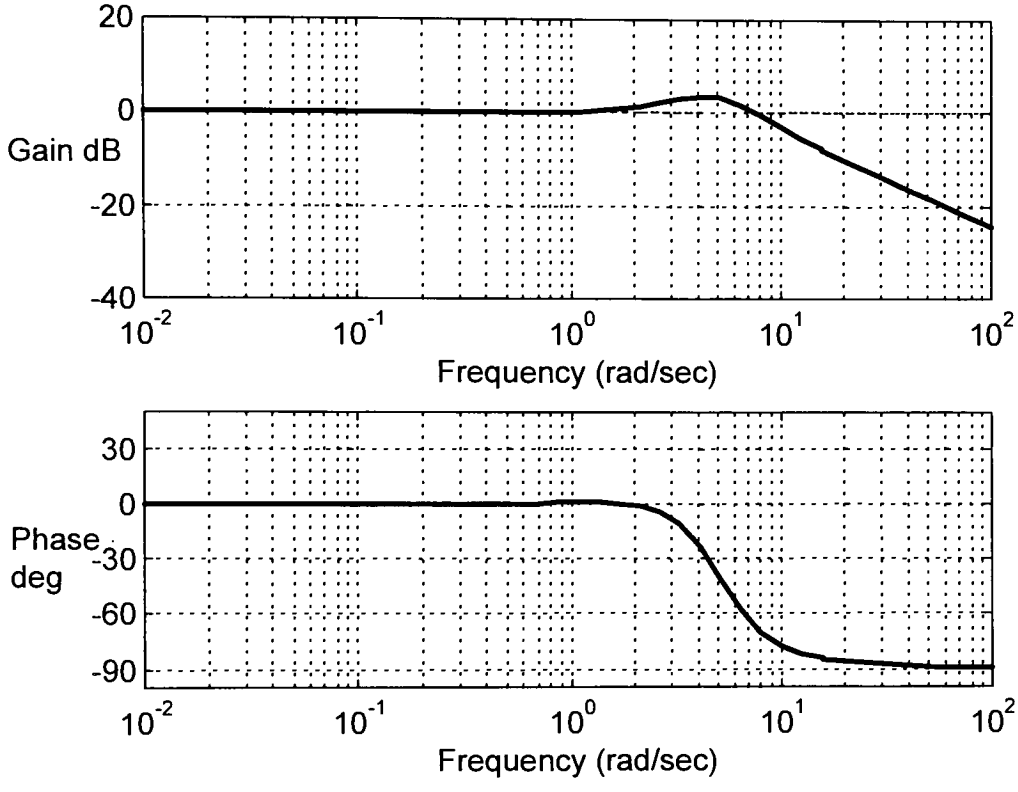

Figure 6 Bode plot of closed-loop system.

Steady-State Error: It is desired for the system to have a zero steady-state error when responding to a step input command in relative lateral position. By including the disturbance D(s) from Fig. 2 and Eqs. (3) - (5) it can be shown that the error signal (command minus actual) E(s) is given by (see Appendix B):

$$E(s) = \frac{y_{rc}s^2 + \left(\frac{V^2}{R}\right)\left(\frac{y_{rc}}{R} - 1\right)}{a_3 s^3 + a_2 s^2 + a_1 s + a_0} \tag{6}$$

where:

$$\begin{aligned} a_3 &= 1 \\ a_2 &= -V K_p \frac{l_2}{L} \\ a_1 &= \frac{V^2}{R^2} - \left(V\frac{l_2}{L}\right)\left(K_i + V\frac{K_p}{l_2}\right) \\ a_0 &= -V^2\frac{K_i}{L} \end{aligned} \tag{7}$$

From the Final Value Theorem, $e_{ss} = e(t=\infty) = \lim_{s\to 0}[sE(s)] = 0$ provided $a_0 = -V^2\frac{K_i}{L} \neq 0$, or $K_i \neq 0$. Therefore, with proportional and integral feedback control action the steady-state error is guaranteed to be zero when tracking a step input. However, it can be shown that the PI controller will not track a ramp with zero steady-state error. To summarize, the controller is classified as a "type I" controller.

Conclusions: A baseline type I PI controller was designed based on a number of standard guidelines such as gain & phase margin and step response parameters including settling time, percent overshoot, steady-state error (of zero) and maximum controller output. It

will serve as a solid benchmark that other controllers can be compared to and / or improved upon.

3.0 Two-Level FLC / PI Controller

Fuzzy logic was first proposed by an American, Lotfi A. Zadeh, in 1965 when he published his seminal paper on "Fuzzy Sets." Zadeh showed that fuzzy logic is the foundation of any logic, regardless of how many truth values it may have. The elements of such sets not only represent the colors black and white, but also allow a spectrum of gray colors in between (Jamshidi M., Vadiee N., and Ross, T., Fuzzy Logic and Control (1993)). Today, application of fuzzy logic *control* (FLC) is widespread, from use in process control, robotics, transportation systems, and other areas. FLC is perhaps the simplest and the most effective control algorithm to use when controlling a system without the aid of a simple mathematical model of the system. Also, another advantage of FLC is that it has the ability to make use of a variety of inputs, unlike conventional controllers that typically accept only one input. The future of FLC is in applying it to real-world applications and in combining it with other control algorithms to improve the performance even further (e.g. neural-fuzzy control algorithms).

Fuzzy logic control has many applications pertaining to the guidance control of vehicles. These applications include: longitudinal control and lateral guidance control of high speed vehicles. Zalila & Lezy (1993) have shown that FLC can be applied to speed regulation and distance control for longitudinal control. Hessburg showed that when considering the lateral guidance control of *high-speed* vehicles the combination of FLC with other control algorithms (e.g. genetic algorithms) performed much better than FLC only, in terms of stability and performance. Guidance applications of FLC also include obstacle avoidance, as in Baxter & Bumby (1994, 1993), autonomous vehicle following

(Kehtarnavan & Nakamura, 1994), and path planning through use of neural-fuzzy control algorithms, (Ro & Lee, 1995).

The focus of this section is on applying a two-level FLC / PI controller to the lateral guidance control of a *low-speed* vehicle. Achieving good performance while only allowing small steering changes is the primary challenge. Small steering angle changes ensure small accelerations which is necessary for passenger comfort and minimization of actuator demands.

For the two-level control system shown in Fig. 8 the PI controller performs the main control action and the fuzzy logic controller monitors the operation and takes action when a change is necessary. In particular, the two-level fuzzy system adjusts the PI controller gains according to certain heuristic rules. This control action is also referred to as gain scheduling of a PI controller using fuzzy logic by Li-Xin Wang in his recent book (1997). Next we will illustrate qualitatively how the FLC rules are to be developed for our problem.

Figure 9 shows an example of a typical time response of our closed-loop system when $y_r(0) = 1$ mm, $\varepsilon(0) = 1$ deg. At the beginning, that is, in the vicinity of point a_1, a large (or "big") control signal is needed in order to achieve a fast rise time. To produce a big control signal, we need large controller gains (both proportional and integral). In the vicinity of point b_1 we would naturally expect a small control signal to avoid a large overshoot, i.e. small controller gains (both proportional and integral). The required control actions around points c_1 and d_1 are similar to those around points a_1 and b_1,

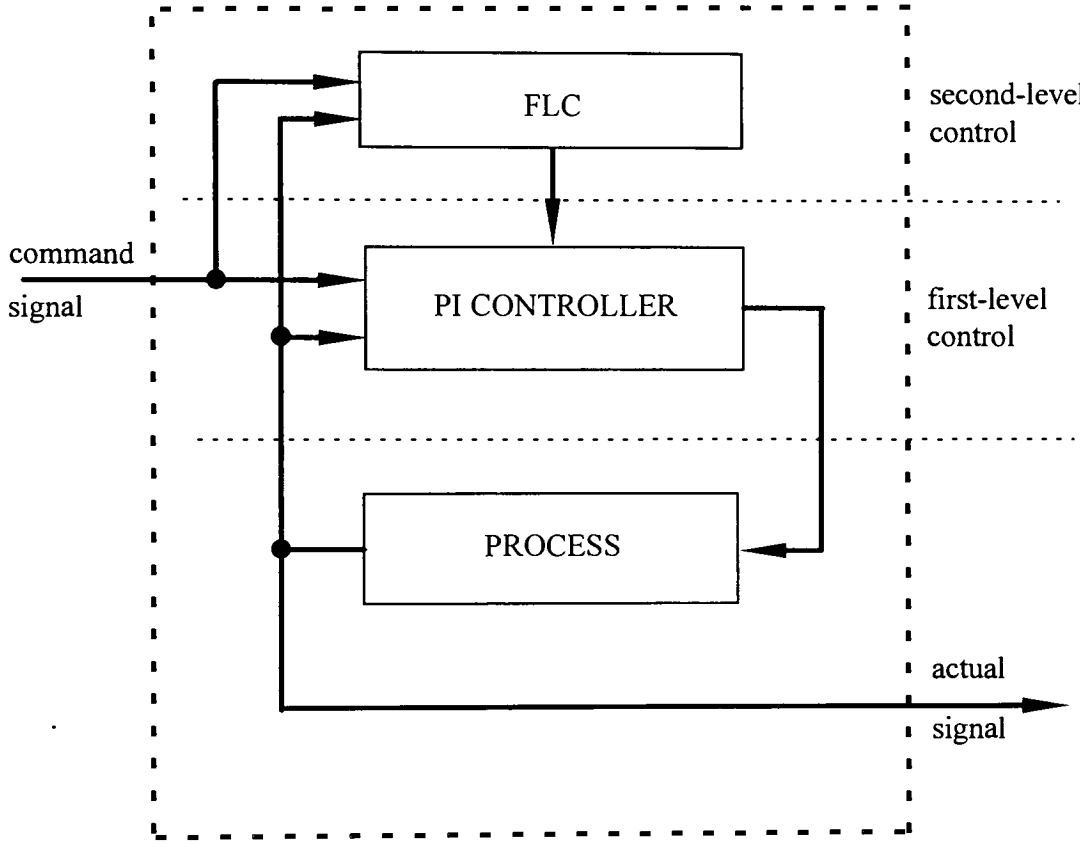

Figure 8 Two-level FLC / PI controller.

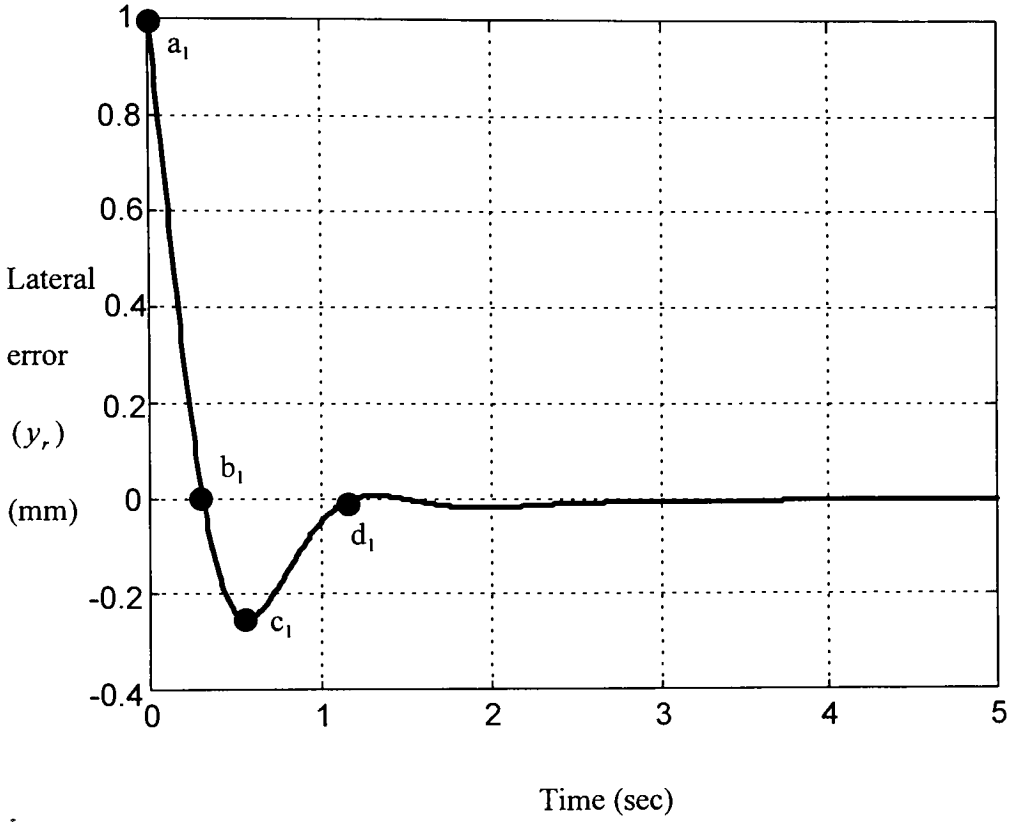

Figure 9 Typical time response of the closed-loop system when $y_r(0) = 1$ mm, $\varepsilon(0) =$ deg.

respectively. It is in this manner that the fuzzy logic control rules are developed and applied to our specific problem.

We will now describe the specific implementation of the two-level FLC / PI controller when applied to the lateral guidance control of a *low-speed* vehicle. A simulation diagram illustrating two-level FLC / PI control of the error-state model is shown in Fig. 10. Three major components of the fuzzy logic control system are: a fuzzifier, a fuzzy rule knowledge base, and a defuzzifier. Converting imprecise or linguistic inputs into fuzzy variables is the function of the fuzzifier. In our case, the lateral error is the only input to the fuzzy logic controller.

The fuzzification process is formalized through the use of membership functions. Figure 11 illustrates the specific symmetric membership functions used. For example, overlapping triangular regions are specified for each of the lateral error membership functions: NEG (negative), ZERO (zero), and POS (positive). The output fuzzy variables are determined by the input variables and application of the three fuzzy rules as defined in Table 1. Basically, if the lateral error (LE) is (not) close to zero, the controller gains are reduced (increased). Proportional (K_p) and integral (K_i) gains are the output variables in this situation. Through defuzzification the output *fuzzy* variables need to be converted to output *crisp* variables for use in control of the physical system; this completes the evaluation of the fuzzy logic control algorithm. The most widely used technique for defuzzification is the "center-of-area technique," which was adopted and found to work satisfactorily in this case. As an interesting aside, note that although a positive integral gain value is clearly not allowed for a stable PI controller with constant gains (from Section 2.0), it is perfectly

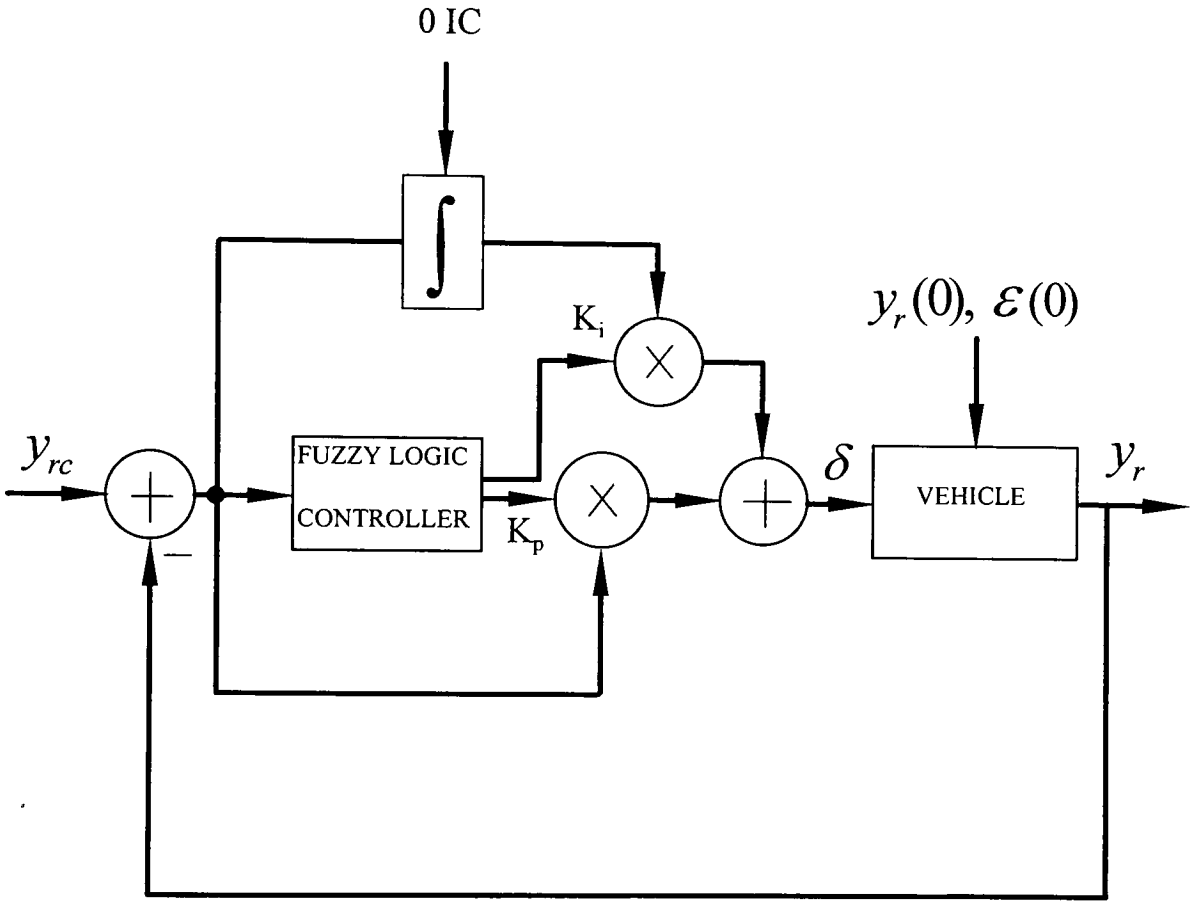

Figure 10 Simulation diagram representation of the two-level FLC / PI controller applied to control of the error-state model.

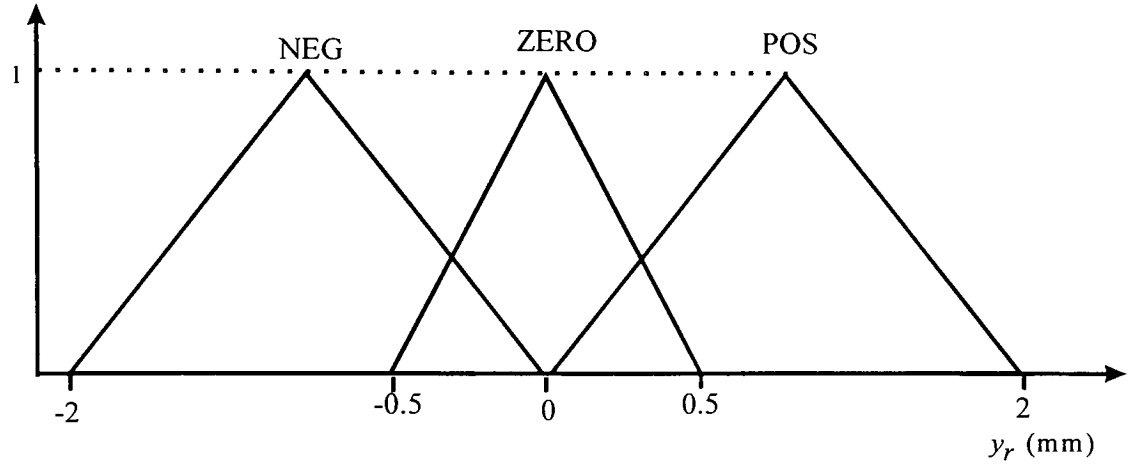

Lateral error (y_r) membership functions

Figure 11 Controller input membership functions.

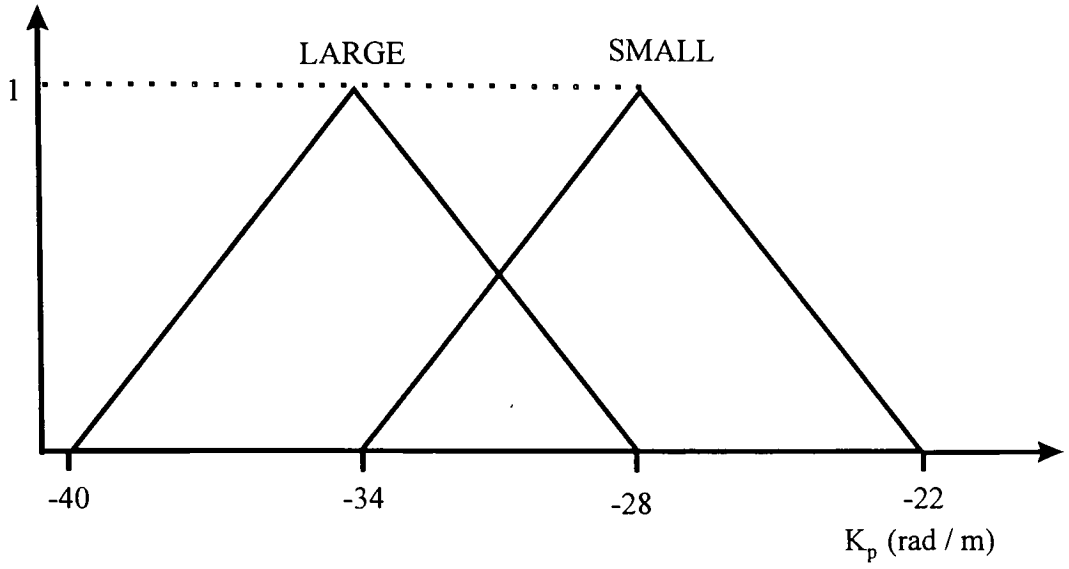

(a) Proportional gain (K_p) membership functions

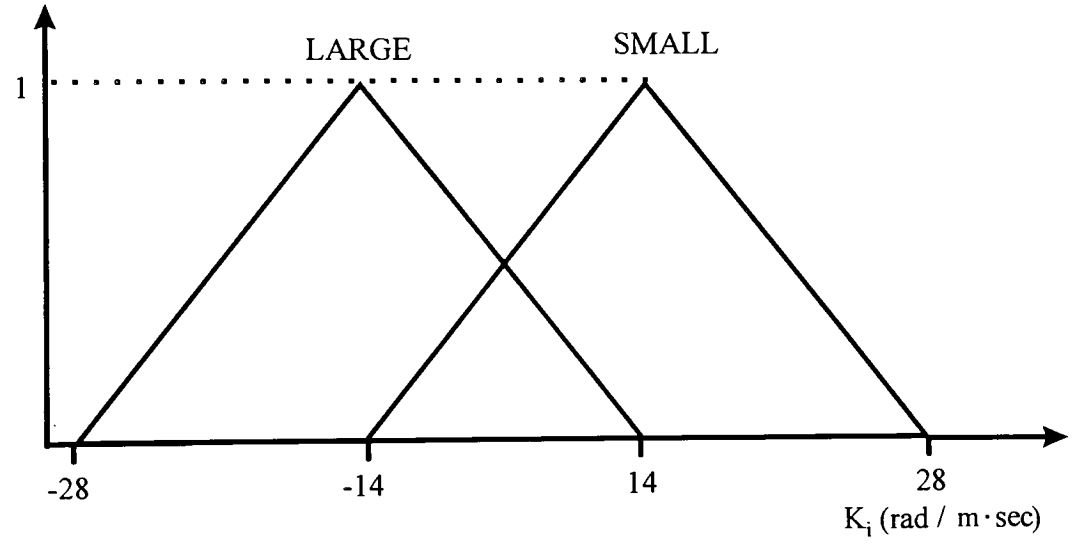

(b) Integral gain (K_i) membership functions

Figure 12 Controller output membership functions.

Table 1 Fuzzy Rules for the Two-Level FLC / PI Controller

RULE NO	INPUT LE	OUTPUT PRGAIN	OUTPUT INGAIN
1	ZERO	SMALL	SMALL
2	NEG	LARGE	LARGE
3	POS	LARGE	LARGE

acceptable to use a positive integral gain value in the membership functions defined in the two-level FLC / PI control algorithm. This is because the positive value will only be in effect for a short period of time. The benefit of allowing sign reversals in the integral feedback gain is that the effect of "integrator wind-up" can be reduced, thereby reducing overshoot and improving the overall performance of the closed-loop system.

To summarize, a two-level FLC / PI controller was designed that is based on three membership functions for lateral error input, two membership functions for proportional gain output, two membership functions for integral gain output, and a total of three fuzzy rules.

4.0 Comparison of PI Controller and Two-Level FLC / PI Controller

4.1 Simulation Issues

To facilitate comparison between the baseline PI controller and the two-level FLC / PI controller the performance of each controller was studied through simulation for a number of specific scenarios. Figure 13 illustrates the general structure of the simulation diagram used; regardless of the controller selected. To eliminate a "kick" (i.e. a jump in δ) due to the lack of feedback initially it was necessary to incorporate a *disturbance cancellation* feedforward term of L / R to the output of the controller (see Eq. (2)).

A total of five simulation scenarios were studied:

- Step response (; $y_{rc}(t) = y_{rc}\mathrm{U}(t)$, $y_r(0) = 0$, $\varepsilon(0) = 0$
- Zero-input response ($y_{rc}(t) = 0$);
  - $y_r(0) = 0$, $\varepsilon(0) = 0$
  - $y_r(0) \neq 0$, $\varepsilon(0) = 0$
  - $y_r(0) = 0$, $\varepsilon(0) \neq 0$
  - $y_r(0) \neq 0$, $\varepsilon(0) \neq 0$

In all cases, the error-state Ackerman steering model from above was used in conjunction with MATLAB® and SIMULINK®. The simulation diagram that realizes the model was implemented in SIMULINK® , see Fig. 14 for the generic simulation diagram and Appendix C for the actual SIMULINK® simulation diagram used. The simulation parameters and initial conditions were selected to support the assumptions; data is

provided in Table 2. A fifth order Runge-Kutta integrator with a minimum (and maximum) time step of 0.01 sec (tolerance 1.0e-3) was found to work satisfactorily when generating a numerical solution.

In addition to MATLAB® / SIMULINK®, the *Fuzzy Logic* TOOLBOX (from The MathWorks, Inc., 1997) was used to permit numerical simulation studies of the above five simulation scenarios. By using the fuzzy inference system (FIS) Editor the FLC controller was built and configured as follows:

- Type : Mamdani
- AND method : Min
- OR Method : Max
- Implication : Product
- Aggregation : Max
- Defuzzification : Centroid

One input and two output variables were selected; three membership functions characterized the input, and two membership functions characterized each of the outputs. To monitor the process and to make sure that all of the appropriate rules are fired by the rule editor (versus default rules), "ruleview" and "surfview" were used and the input intervals were changed as necessary using "mfedit." Finally, the "fuzblock" utility was invoked from within MATLAB® to permit incorporation of the FLC directly into SIMULINK® (represented as a simulation block) and interfacing with the plant which was modeled using simulation blocks as discussed in Sahin (1997).

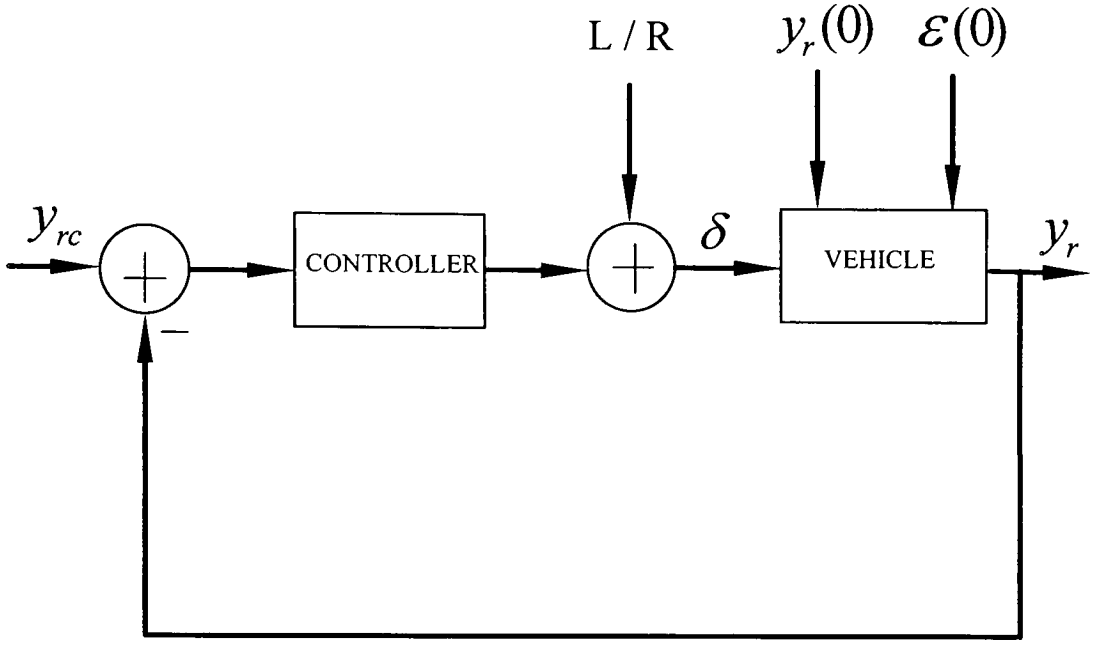

Figure 13 Simulation diagram representation of control of the error-state model (with disturbance cancellation).

Table 2 Simulation Parameters and Scenarios

Parameters

R = 10 m

L = 0.30 m

l_2 = 0.12 m

V = 0.5 m / sec
(not critical)

Scenarios

No	$y_{rc}(0)$ (mm)	$y_r(0)$ (mm)	$\varepsilon(0)$ (deg)
1	U(t)	0	0
2	0	0	0
3	0	1	0
4	0	0	1
5	0	1	1

4.2 Simulation Results and Comparison

For each of the above scenarios the baseline PI controller was compared to the two-level FLC / PI controller by monitoring the following quantities:

- Overshoot
- Settling time t_s
- Realistic controller output (steering input) δ

Assuming that the controller output is within an acceptable range, the primary concern is overshoot and settling time of the response $y_r(t)$. Table 3 summarizes the major results of the simulations. Relevant simulation results for each of the scenarios is shown in Figs. 14 - 23, including lateral error and steering input time responses.

Overshoot: For each of the simulations performed the two-level FLC / PI controller performed at least slightly better with respect to overshoot. In the case of a step input (i.e. scenario # 1) the overshoot M_p was reduced from 30 % to 20 %, small but an improvement. For each of the zero-input response cases considered (scenario #'s 2-5), the improvement in overshoot was more noticeable, especially after the second peak of the response, typically a 50-100 % reduction.

Settling Time: In general the settling time t_s (5 % criterion) was reduced for each of the scenarios simulated when using the two-level FLC / PI controller. For the standard case of a step input (i.e. scenario #1) the settling time was reduced by 21 % when compared to

the baseline PI controller. Similarly, the zero-input response cases (scenario #'s 2-5) produce a reduction in the settling time in the range of 22-60 %[3].

Controller Output / Steering Input: In all of the scenarios simulated there was an improvement in the steered wheel angle response $\delta(t)$ when using the two-level FLC / PI controller, versus the baseline PI controller. Peak reductions in $|\delta|$ were observed (see Figs. 15, 17, 19, 21, and 23. This will increase the comfort level of the passengers on-board the vehicle.

[3] For the zero-input response case, the *settling time* is defined as the smallest time at which the response continues to remain within 0.02 mm of the steady-state value of 0 mm.

Table 3 Settling and overshoot of controllers for five scenarios

Scenarios	Overshoot (mm)		Settling Time (sec)	
No	Two-Level FLC / PI Controller	PI Controller	Two-Level FLC / PI Controller	PI Controller
1	1.2	1.3	1.1	1.4
2	0.0	0.2	1.4	3.1
3	0.0	0.2	1.4	2.6
4	0.0	0.1	1.2	3.0
5	0.1	0.2	1.4	1.8

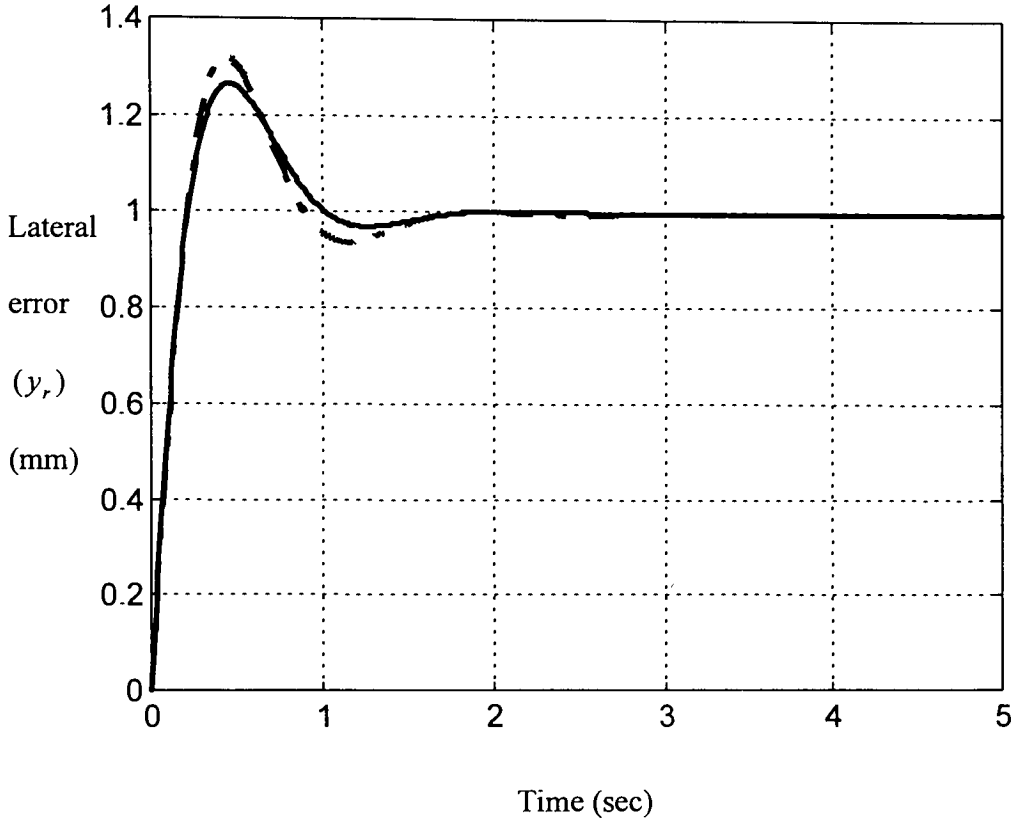

Figure 14 Simulation for step response (scenario # 1). Note: the FLC / PI controller response is represented by a solid line (-) and the conventional PI controller response is represented by a dashed line (--).

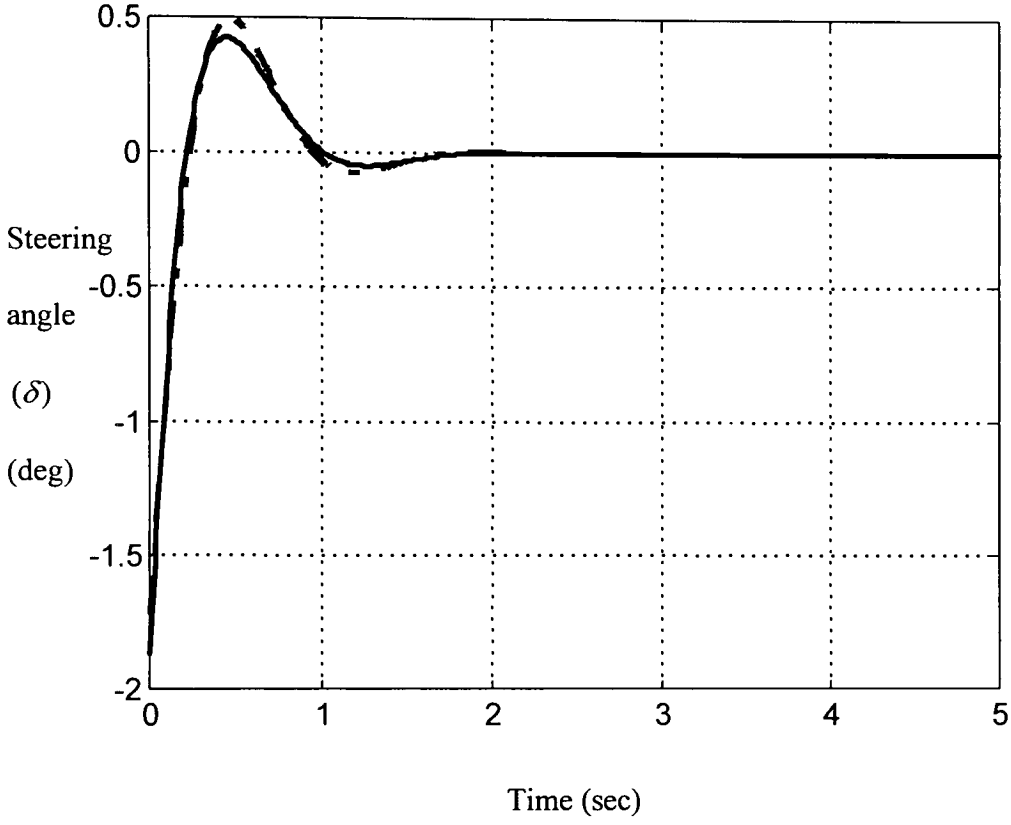

Figure 15 Simulation for step response (scenario # 1). Note: the FLC / PI controller response is represented by a solid line (-) and the conventional PI controller response is represented by a dashed line (--).

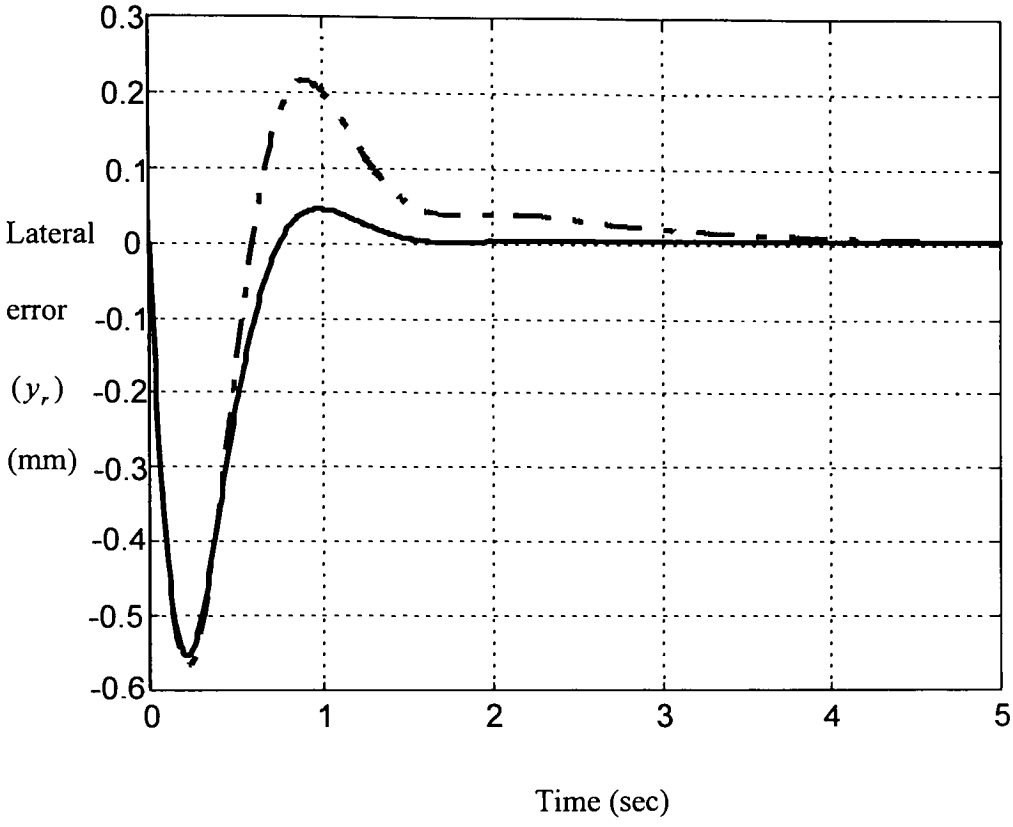

Figure 16 Simulation for $y_r(0) = 0$ mm, $\varepsilon(0) = 0$ deg (scenario # 2). Note: (1) the two-level FLC / PI controller response is represented by a solid line (-) and the conventional PI controller response is represented by a dashed line (--), (2) the transient response exists because δ = L / R cancels the disturbance but not $\dot{y}_r(0)$.

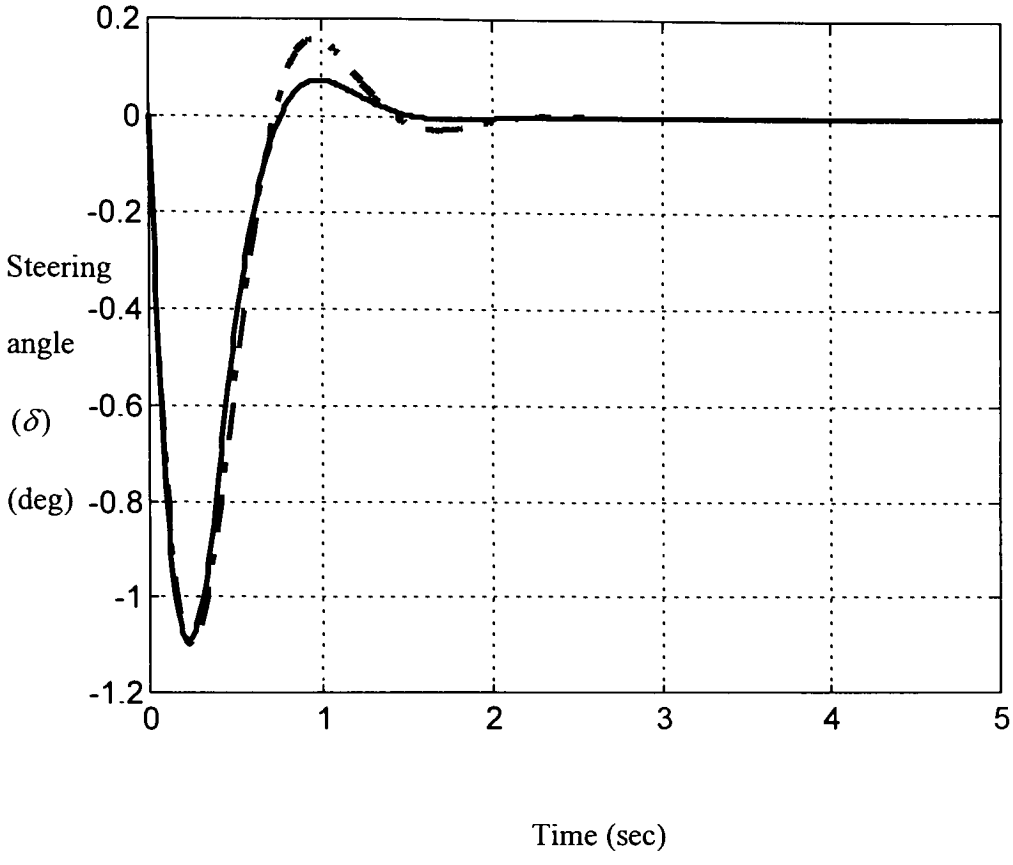

Figure 17 Simulation for $y_r(0) = 0$ mm, $\varepsilon(0) = 0$ deg (scenario # 2). Note: (1) the FLC / PI controller response is represented by a solid line (-) and the conventional PI controller response is represented by a dashed line (--), (2) the transient response exists because $\delta = \mathrm{L} / \mathrm{R}$ cancels the disturbance but not $\dot{y}_r(0)$.

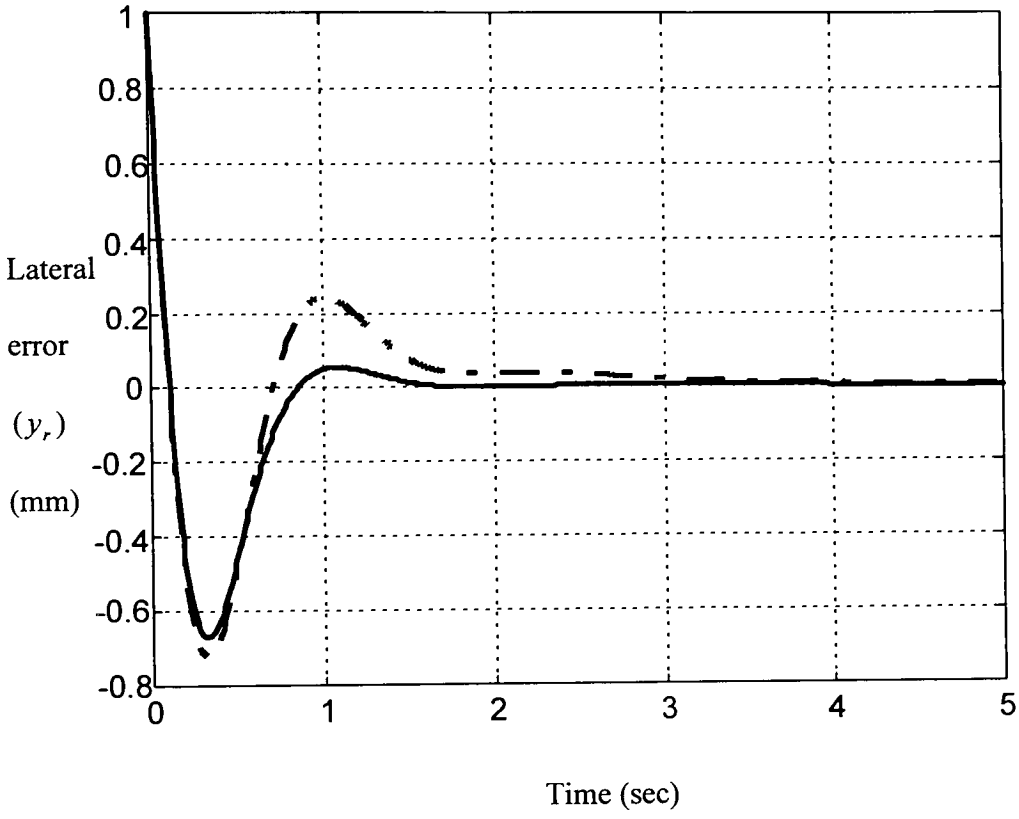

Figure 18 Simulation for $y_r(0) = 1$ mm, $\varepsilon(0) = 0$ deg (scenario # 3). Note: the FLC / PI controller response is represented by a solid line (-) and the conventional PI controller response is represented by a dashed line (--).

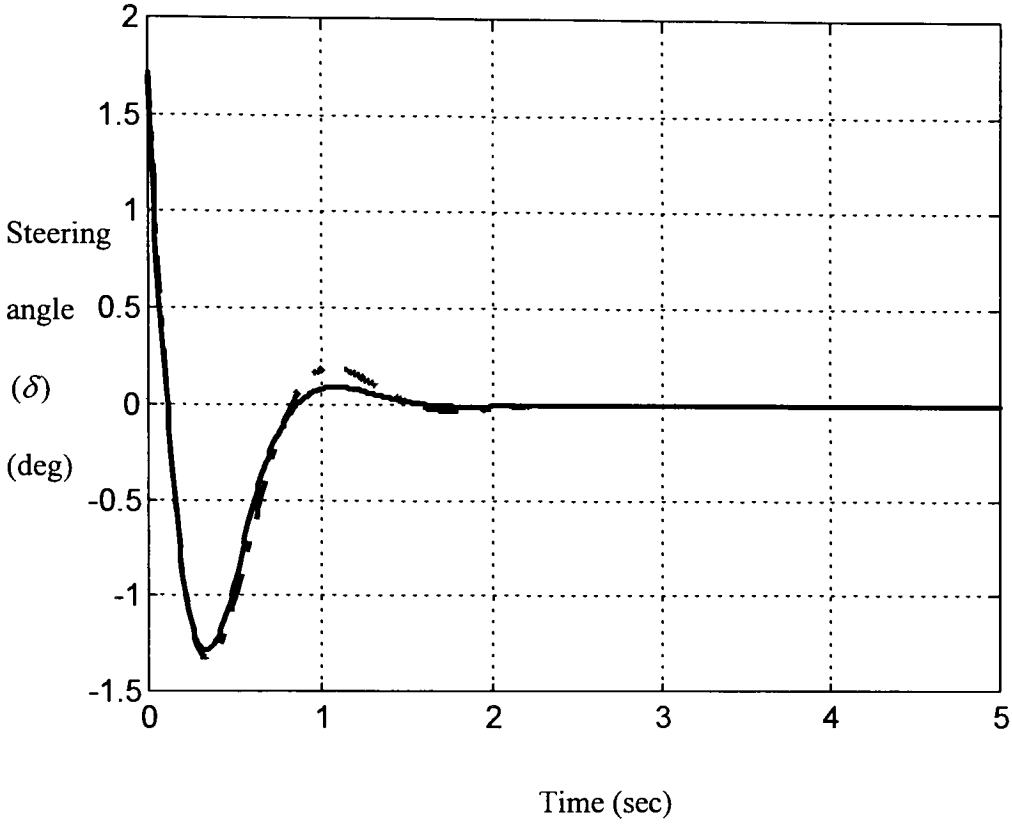

Figure 19 Simulation for $y_r(0) = 1$ mm, $\varepsilon(0) = 0$ deg (scenario # 3). Note: the two-level FLC / PI controller response is represented by a solid line (-) and the conventional PI controller response is represented by a dashed line (--).

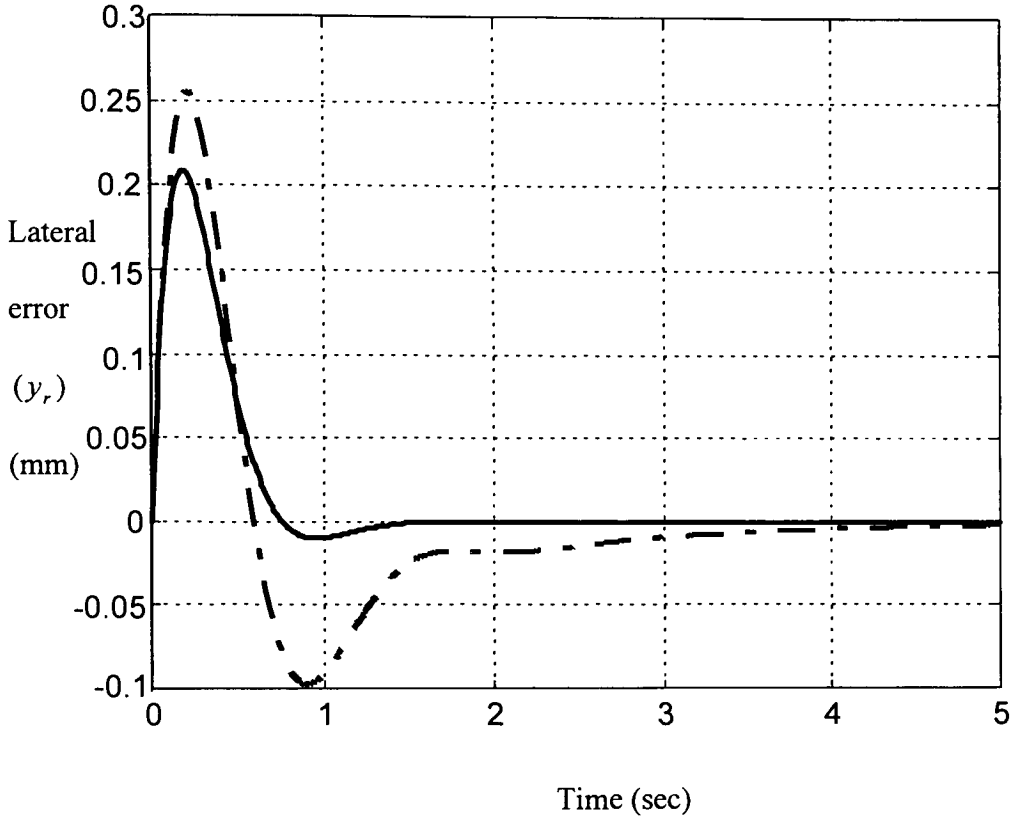

Figure 20 Simulation for $y_r(0) = 0$ mm, $\varepsilon(0) = 1$ deg (scenario # 4). Note: the FLC / PI controller response is represented by a solid line (-) and the conventional PI controller response is represented by a dashed line (--).

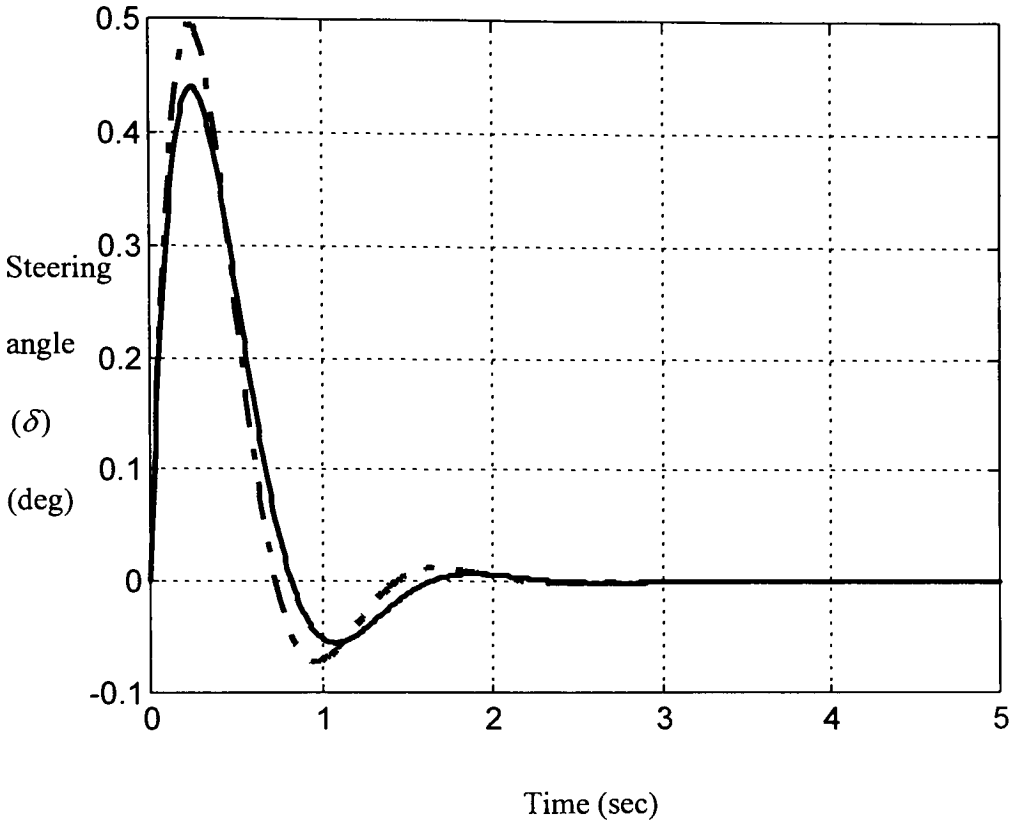

Figure 21 Simulation for $y_r(0) = 0$ mm, $\varepsilon(0) = 1$ deg (scenario # 4). Note: the FLC / PI controller response is represented by a solid line (-) and the conventional PI controller response is represented by a dashed line (--).

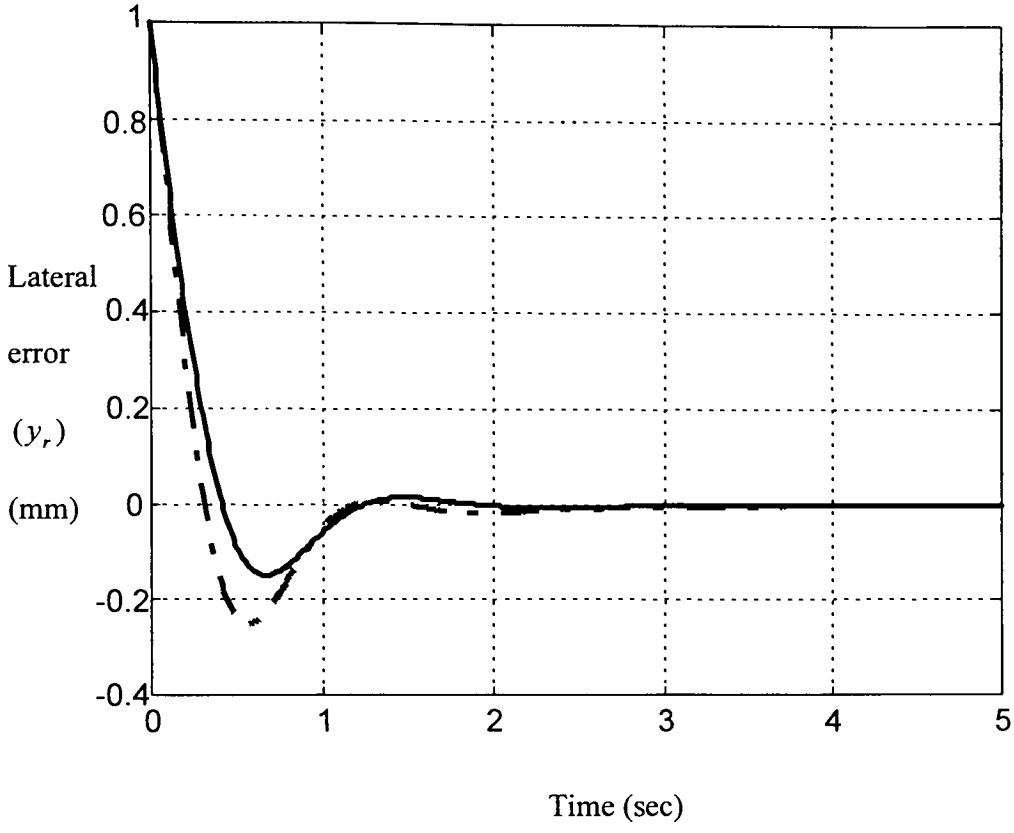

Figure 22 Simulation for $y_r(0) = 1$ mm, $\varepsilon(0) = 1$ deg (scenario # 5). Note: the FLC / PI controller response is represented by a solid line (-) and the conventional PI controller response is represented by a dashed line (--).

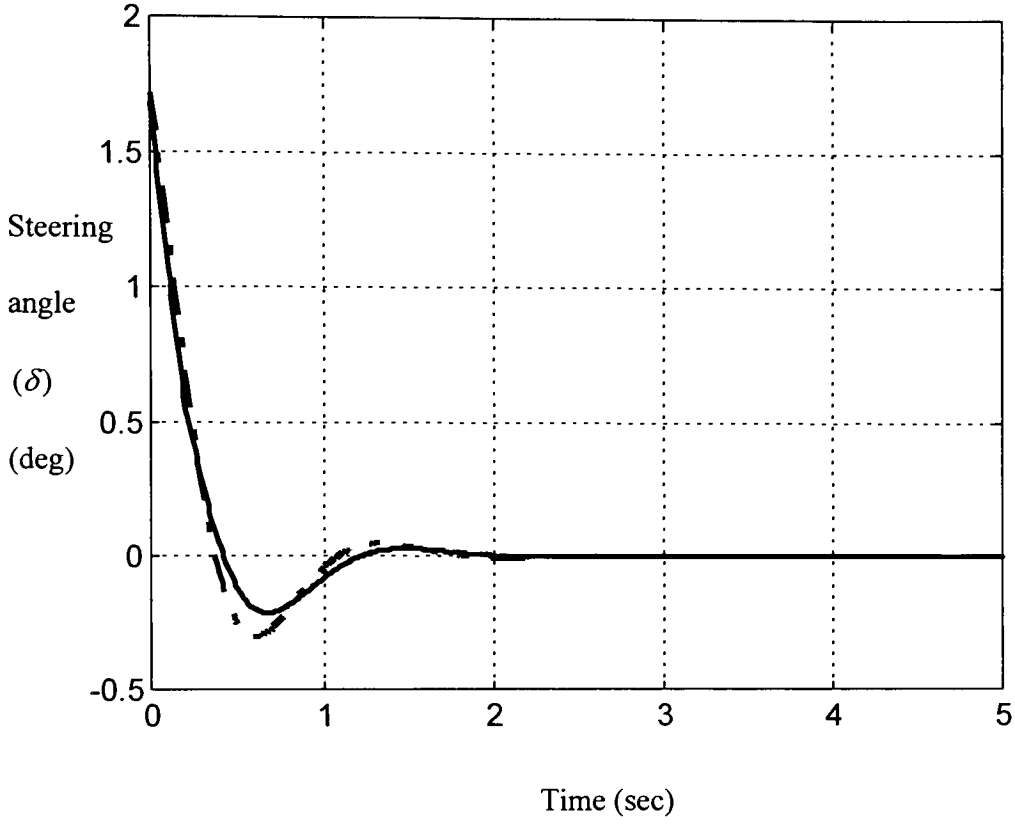

Figure 23 Simulation for $y_r(0) = 1$ mm, $\varepsilon(0) = 1$ deg (scenario # 5). Note: the FLC / PI controller response is represented by a solid line (-) and the conventional PI controller response is represented by a dashed line (--).

5.0 Conclusions

A "baseline PI controller" and a two-level FLC / PI controller were designed for use in lateral guidance control of a vehicle traversing at low speeds. The plant is characterized as a linear nonminimum-phase "error-state" bicycle model based on Ackerman steering. The baseline PI controller was designed using classical control techniques and the fuzzy logic controller is characterized as a two-level FLC / PI controller utilizing three membership functions for lateral error input, two membership functions each for proportional gain and integral feedback gains, and a total of three fuzzy rules. Gain ranges for the two-level FLC / PI controller overlap those used in the baseline PI controller. Simulations were created in MATLAB® / SIMULINK® and used to permit comparison between the baseline PI controller and the two-level FLC / PI controller. In general the two-level FLC / PI controller always performed at least as well as the baseline PI controller when measured using such performance metrics as overshoot and settling time. There were instances when a 60 % reduction in effective settling time and a 100 % reduction in effective overshoot (second peak) were realized. In conclusion, we have shown that both a classical PI controller and a two-level FLC / PI controller offer potential for high performance control of low-speed vehicles exhibiting Ackerman steering characteristics.

6.0 Acknowledgments

The author wishes to acknowledge the Turkish Republic's Ministry of National Education for partial support of this work.

References

1. Baxter, J. W. and Bumby, J. R. "Fuzzy Control of a mobile Robotic Vehicle," Proceedings of the Institution of Mechanical Engineers. Part 1, Journal of Systems & Control Engineering v 209 n2 1994 MEP Edmunds Engl. P 79-91.

2. Frankel, J., Alvarez, L., Horowitz, R., and Li, P., "Safety Oriented Maneuvers for IVHS," *Vehicle System Dynamics*, 26 (1996), pp. 271-299.

3. Hessburg, T. M., "Fuzzy Logic Control with Adaptive Methods for Vehicle Lateral Guidance," PhD. Dissertation, University of California at Berkeley, 1994.

4. Kehternavaz, N., Nakamura, E., Griswold, N. and Yen, J. "Autonomous Vehicle Following by a Fuzzy Logic Controller," Proceedings of the 1994 1st International Joint Conference of NAFIPS / IFIS / NASA Dec 18-21 1994 San Antonio, TX, USA sponsored by IEEE p 333-337.

5. Kuo, C. B., *Automatic Control Systems*. Seventh Edition, Prentice Hall, Inc. 1995.

6. Jamshidi M., Vadiee N., and Ross, T., *Fuzzy Logic and Control.* Prentice Hall PTR, 1993.

7. Ogata K., *Modern Control Theory*. Third Edition, Prentice Hall, Inc., 1997.

8. Pears, N. E. And Bumby, J. R., "Guidance of an autonomous guided vehicle using low-level ultrasonic and odometry sensor systems," Trans Inst MC, Vol 11 No 5, Oct.-Dec. 1989.

9. Peng, H. and Tomizuka, M., "Preview Control for Vehicle Lateral Guidance in Highway Automation," ASME *Journal of Dynamic Systems, Measurement, and Control,* December 1993, Vol. 115, pp. 679-686.

10. Ro, Paul J. and Lee, B. R. "Neural-Fuzzy Hybrid System for Mobile Robot Path-Planning in a Partially Known Environment," Proceedings of the 1995 American Control Conference Part 1 (of 6) Jun 21-23 v 1 Seattle, WA, USA sponsored by AACC 6 p 673-677.

11. Sahin, H., "Lateral Guidance Control of a Low-Speed Vehicle," MS Thesis, Rochester Institute of Technology, 1997.

12. The MathWorks, Inc., "*Fuzzy Logic* TOOLBOX, for use with MATLAB®," Natick, MA, January 1995.

13. The MathWorks, Inc., "MATLAB® Reference Guide, High-Performance Numeric Computation and Visualization Software," Natick, MA, July 1993.

14. The MathWorks, Inc., "SIMULINK® User's Guide, Dynamic System Simulation Software, For Microsoft Windows," Natick, MA, June 1995.

15. Wang, Li-Xin, *A Course in Fuzzy Systems and Control*. Prentice Hall PTR, 1997.

16. Wong, J. Y., *Theory of Ground Vehicles*. John Wiley & Sons, Inc. 1993.

17. Zalila, Z. and Lezy, P., "Longitudinal Control of an Autonomous Vehicle Through a Hybrid Fuzzy / Classical Controller," Proceedings of the 1994 Wescon Conference Sep 27-29 1994 Anaheim, CA, USA sponsored by IEEE p 118-124.

Appendix A Transfer Function Derivation of Plant

Laplace transform of state equations ($y_r(0) = 0,\ \varepsilon(0) = 0$):

$$Y_r(s)s = V\varepsilon(s) - \frac{l_2}{L}V\Delta(s) \tag{A-1}$$

$$\varepsilon(s)s = -V\frac{Y_r(s)}{R^2} - V\frac{\Delta(s)}{L} + \frac{V}{R}\frac{1}{s} \tag{A-2}$$

Solution for response in Laplace domain $Y_r(s)$:

$$\varepsilon = -\frac{V}{R^2}\frac{Y_r(s)}{s} - \frac{V}{L}\frac{\Delta(s)}{s} + \frac{V}{Rs^2} \tag{A-3}$$

$$Y_r(s)s = V\left(-\frac{V}{R^2}\frac{Y_r(s)}{s} - \frac{V}{L}\frac{\Delta(s)}{s} + \frac{V}{Rs^2}\right) - \frac{l_2}{L}V\Delta(s) \tag{A-4}$$

$$Y_r(s)\left(s + \frac{V^2}{sR^2}\right) = -\frac{V^2}{L}\frac{\Delta(s)}{s} + \frac{V^2}{Rs^2} - \frac{l_2}{L}V\Delta(s) \tag{A-5}$$

$$Y_r(s) = \frac{\left(-\frac{Vl_2}{L}\right)\left(s + \frac{V}{l_2}\right)}{s^2 + \frac{V^2}{R^2}}\Delta(s) + \frac{\frac{V^2}{R}}{s\left(s^2 + \frac{V^2}{R^2}\right)} \equiv G_p(s)\Delta(s) + D(s) \tag{A-6}$$

Appendix B Steady-State Error Calculation

$$G_c = K_p + \frac{K_i}{s} + K_d s \tag{B-1}$$

$$E(s) = Y_{rc}(s) - Y_r(s) \tag{B-2}$$

$$\Delta(s) = G_c E(s) \equiv \left(K_p + \frac{K_i}{s} + K_d s \right) E(s) \tag{B-3}$$

$$Y_r(s) = G_c G_p E(s) + D(s) \; = G_c G_p Y_{rc}(s) - G_c G_p Y_r(s) + D(s) \tag{B-4}$$

$$\therefore \; Y_r(s) = \frac{G_c G_p}{1 + G_c G_p} Y_{rc}(s) + \frac{D(s)}{1 + G_c G_p} \tag{B-5}$$

If $Y_{rc}(s) = \frac{y_{rc}}{s}$ (step input command) then we want $e_{ss} = e(t = \infty) = 0$,

$$Y_r(s) = \frac{G_c G_p}{1 + G_c G_p} \left(\frac{y_{rc}}{s} \right) + \frac{D(s)}{1 + G_c G_p} \tag{B-6}$$

$$E(s) = \frac{y_{rc}}{s} - \frac{G_c G_p}{1 + G_c G_p} \left(\frac{y_{rc}}{s} \right) - \frac{D(s)}{1 + G_c G_p} \tag{B-7}$$

so that

$$E(s) = \frac{1}{1 + G_c G_p} \left(\frac{y_{rc}}{s} - D \right) \tag{B-8}$$

From the Final Value Theorem, the steady-state error, e_{ss} is given by:

$$e_{ss} = \lim_{s \to 0} [sE(s)] = \lim_{s \to 0} \left[\frac{s}{1 + G_c G_p} \left(\frac{y_{rc}}{s} - D \right) \right] \tag{B-9}$$

where,

$$1+G_cG_p = 1+\frac{\left(-\frac{Vl_2}{L}\right)\left(s+\frac{V}{l_2}\right)}{s^2+\frac{V^2}{R^2}}\left(K_p+\frac{K_i}{s}+K_ds\right) \tag{B-10}$$

Rewriting and simplifying,

$$1+G_cG_p = \frac{s\left(s^2+\frac{V^2}{R^2}\right)-\left(\frac{Vl_2}{L}\right)\left(s+\frac{V}{l_2}\right)\left(K_ps+K_i+K_ds^2\right)}{s\left(s^2+\frac{V^2}{R^2}\right)} \tag{B-11}$$

$$= \frac{s^3+\left(\frac{V^2}{R^2}\right)s-\left(\frac{Vl_2}{L}\right)\left(K_ps^2+K_is+K_ds^3+\left(V\frac{K_p}{l_2}\right)s+V\frac{K_i}{l_2}+K_d\left(\frac{V}{l_2}\right)s^2\right)}{s\left(s^2+\frac{V^2}{R^2}\right)} \tag{B-12}$$

$$= \frac{s^3+\left(\frac{V^2}{R^2}\right)s-\left(\frac{Vl_2}{L}\right)\left(K_ds^3+\left(K_p+V\frac{K_d}{l_2}\right)s^2+\left(K_i+V\frac{K_p}{l_2}\right)s+V\frac{K_i}{l_2}\right)}{s\left(s^2+\frac{V^2}{R^2}\right)} \tag{B-13}$$

$$= \frac{\left(1-\frac{VK_dl_2}{L}\right)s^3-\left(\frac{Vl_2}{L}\right)\left(K_p+V\frac{K_d}{l_2}\right)s^2+\left(\frac{V^2}{R^2}-\frac{Vl_2}{L}\left(K_i+V\frac{K_p}{l_2}\right)\right)s-V^2\frac{K_i}{L}}{s^3+\frac{V^2}{R^2}s} \tag{B-14}$$

so that the first factor in Eq. (B-9) is:

$$\frac{s}{1+G_c G_p} = \frac{s^2\left(s^2 + \frac{V^2}{R^2}\right)}{a_3 s^3 + a_2 s^2 + a_1 s + a_0} \tag{B-15}$$

where:

$$a_3 = \left(1 - \frac{V K_d l_2}{L}\right),\ a_2 = -\left(\frac{V l_2}{L}\right)\left(K_p + V\frac{K_d}{l_2}\right) \tag{B-16}$$

$$a_1 = \frac{V^2}{R^2} - \frac{V l_2}{L}\left(K_i + V\frac{K_p}{l_2}\right),\ a_0 = -V^2\frac{K_i}{L} \tag{B-17}$$

Evaluating the remaining factor needed in Eq. (B-9) yields:

$$\frac{y_{rc}}{s} - D = \frac{y_{rc}}{s} - \frac{\left(\frac{V^2}{R}\right)}{s\left(s^2 + \frac{V^2}{R^2}\right)} \tag{B-18}$$

$$= \frac{y_{rc}\left(s^2 + \frac{V^2}{R^2}\right) - \frac{V^2}{R}}{s\left(s^2 + \frac{V^2}{R^2}\right)} \tag{B-19}$$

$$= \frac{y_{rc}s^2 + \left(\frac{V^2}{R}\right)\left(\frac{y_{rc}}{R} - 1\right)}{s\left(s^2 + \frac{V^2}{R^2}\right)} \tag{B-20}$$

so that sE(s) is given by:

$$= \frac{s^2\left(s^2 + \frac{V^2}{R^2}\right)}{a_3 s^3 + a_2 s^2 + a_1 s + a_0} \frac{y_{rc} s^2 + \left(\frac{V^2}{R}\right)\left(\frac{y_{rc}}{R} - 1\right)}{s\left(s^2 + \frac{V^2}{R^2}\right)} \tag{B-21}$$

$$= \frac{y_{rc} s^3 + \left(\frac{V^2}{R}\right)\left(\frac{y_{rc}}{R} - 1\right)s}{a_3 s^3 + a_2 s^2 + a_1 s + a_0} \tag{B-22}$$

Therefore,

$$e_{ss} = \lim_{s \to 0}\left[sE(s)\right] = 0 \text{ provided } a_0 \neq 0$$

Recall that

$$a_0 = \left(-\frac{V^2}{L}\right)K_i \Rightarrow \boxed{e_{ss} = 0 \text{ if } K_i \neq 0} \tag{B-23}$$

Appendix C: SIMULINK® Simulation Diagrams

Baseline PI Controller Simulation Diagram

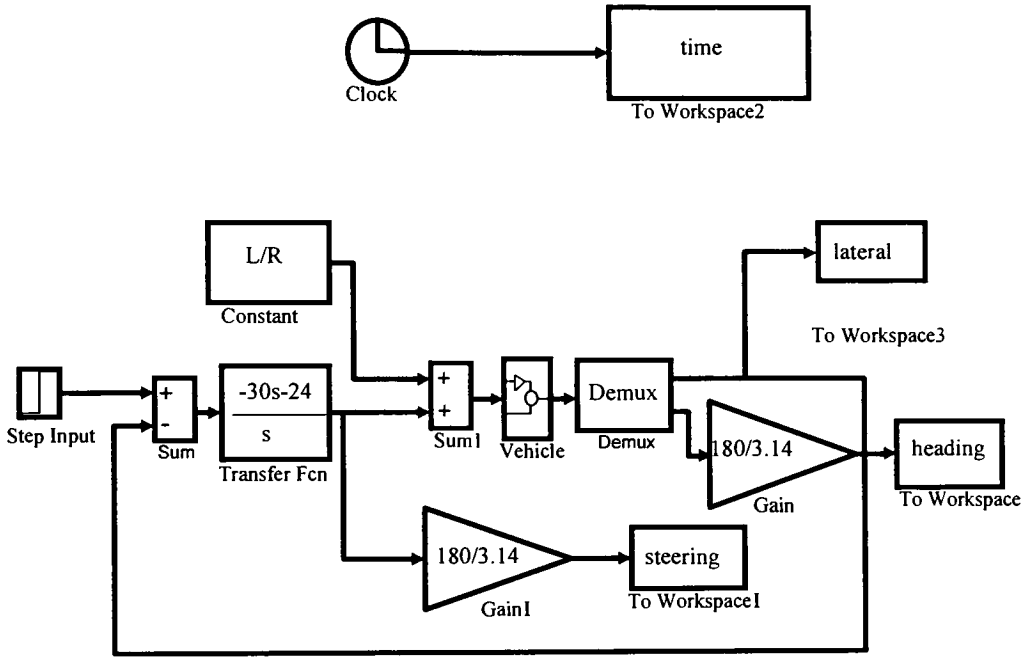

Vehicle Subsystem

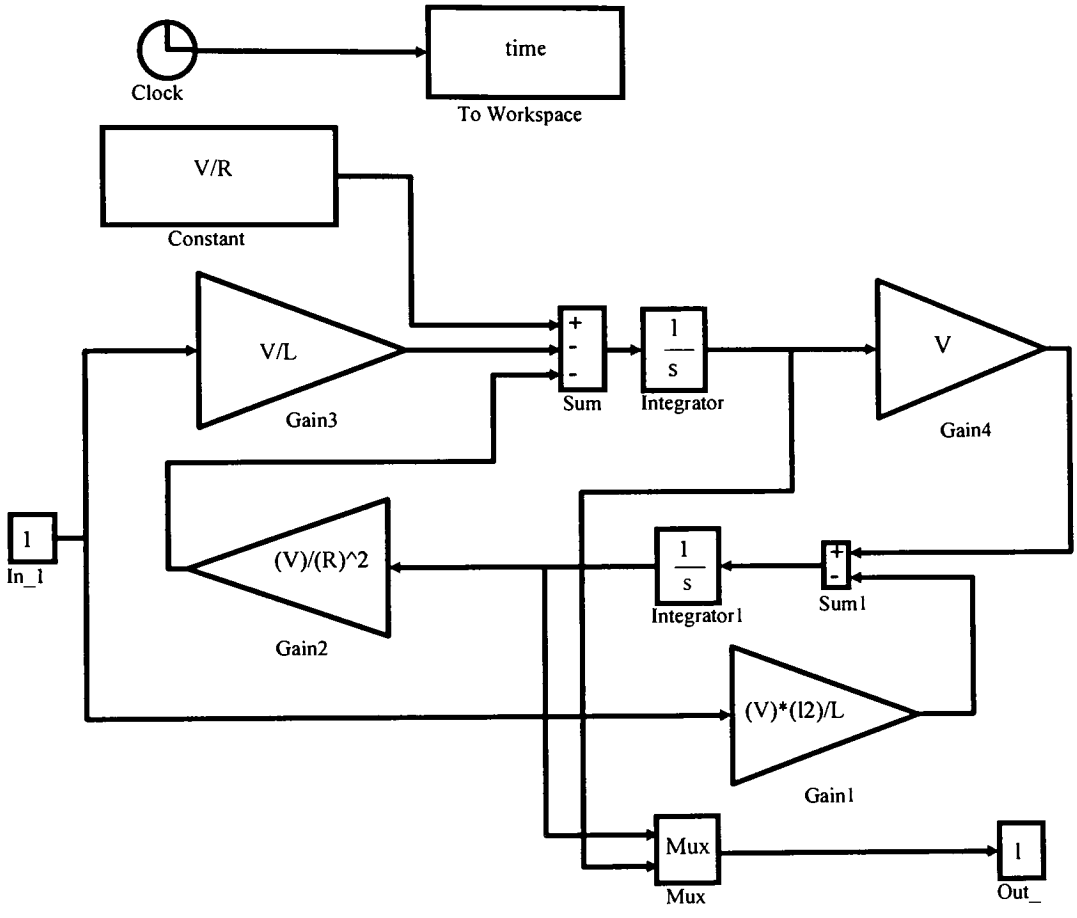

Two-Level FLC / PI Controller Simulation Diagram